PHYSICAL REVIEW D **95,** 043541 (2017)

Ultralight scalars as cosmological dark matter

Lam Hui[*]
Department of Physics, Columbia University, New York, New York 10027, USA

Jeremiah P. Ostriker[†]
Department of Astronomy, Columbia University, New York, New York 10027, USA
and Department of Astrophysical Sciences, Princeton University, Princeton, New Jersey 08544, USA

Scott Tremaine[‡] and Edward Witten[§]
Institute for Advanced Study, Princeton, New Jersey 08540, USA
(Received 28 October 2016; published 28 February 2017)

Many aspects of the large-scale structure of the Universe can be described successfully using cosmological models in which $27 \pm 1\%$ of the critical mass-energy density consists of cold dark matter (CDM). However, few—if any—of the predictions of CDM models have been successful on scales of ~ 10 kpc or less. This lack of success is usually explained by the difficulty of modeling baryonic physics (star formation, supernova and black-hole feedback, etc.). An intriguing alternative to CDM is that the dark matter is an extremely light ($m \sim 10^{-22}$ eV) boson having a de Broglie wavelength $\lambda \sim 1$ kpc, often called fuzzy dark matter (FDM). We describe the arguments from particle physics that motivate FDM, review previous work on its astrophysical signatures, and analyze several unexplored aspects of its behavior. In particular, (i) FDM halos or subhalos smaller than about $10^7 (m/10^{-22}\ \mathrm{eV})^{-3/2}\ M_\odot$ do not form, and the abundance of halos smaller than a few times $10^{10} (m/10^{-22}\ \mathrm{eV})^{-4/3}\ M_\odot$ is substantially smaller in FDM than in CDM. (ii) FDM halos are comprised of a central core that is a stationary, minimum-energy solution of the Schrödinger-Poisson equation, sometimes called a "soliton," surrounded by an envelope that resembles a CDM halo. The soliton can produce a distinct signature in the rotation curves of FDM-dominated systems. (iii) The transition between soliton and envelope is determined by a relaxation process analogous to two-body relaxation in gravitating N-body systems, which proceeds as if the halo were composed of particles with mass $\sim \rho\lambda^3$ where ρ is the halo density. (iv) Relaxation may have substantial effects on the stellar disk and bulge in the inner parts of disk galaxies, but has negligible effect on disk thickening or globular cluster disruption near the solar radius. (v) Relaxation can produce FDM disks but a FDM disk in the solar neighborhood must have a half-thickness of at least $\sim 300 (m/10^{-22}\ \mathrm{eV})^{-2/3}$ pc and a midplane density less than $0.2 (m/10^{-22}\ \mathrm{eV})^{2/3}$ times the baryonic disk density. (vi) Solitonic FDM subhalos evaporate by tunneling through the tidal radius and this limits the minimum subhalo mass inside ~ 30 kpc of the Milky Way to a few times $10^8 (m/10^{-22}\ \mathrm{eV})^{-3/2}\ M_\odot$. (vii) If the dark matter in the Fornax dwarf galaxy is composed of CDM, most of the globular clusters observed in that galaxy should have long ago spiraled to its center, and this problem is resolved if the dark matter is FDM. (viii) FDM delays galaxy formation relative to CDM but its galaxy-formation history is consistent with current observations of high-redshift galaxies and the late reionization observed by *Planck*. If the dark matter is composed of FDM, most observations favor a particle mass $\gtrsim 10^{-22}$ eV and the most significant observational consequences occur if the mass is in the range $1\text{–}10 \times 10^{-22}$ eV. There is tension with observations of the Lyman-α forest, which favor $m \gtrsim 10\text{–}20 \times 10^{-22}$ eV and we discuss whether more sophisticated models of reionization may resolve this tension.

DOI: 10.1103/PhysRevD.95.043541

I. INTRODUCTION

The standard lambda cold dark matter (ΛCDM) model for the mass-energy content of the Universe and the development of cosmic structure has been remarkably successful. In this model the Universe is geometrically flat and the largest contributors to the mass-energy are dark energy, $68 \pm 1\%$ of the total, and dark matter, $27 \pm 1\%$ [1], both of unknown nature. Most likely the dark matter consists of some undiscovered elementary particle(s), produced early in the history of the Universe, that is "cold" in the sense that the effect of its velocity dispersion on structure formation is negligible. Ordinary or baryonic

[*]lhui@astro.columbia.edu
[†]ostriker@princeton.edu
jpo@astro.columbia.edu
[‡]tremaine@ias.edu
[§]witten@ias.edu

matter is a minor constituent (5%), and neutrinos and other light or zero-mass particles make an even smaller contribution to the total mass-energy density. This mixture of components, with small density fluctuations normalized to the observed fluctuations in the cosmic microwave background radiation field and allowed to grow via gravitational instabilities, can account for the properties of the structures in the Universe at most well-observed scales and epochs. The initial spectral index of the perturbations is slightly less than unity, $n_s = 0.965 \pm 0.006$, consistent with simple theories in which the Universe passes through an early inflationary stage. N-body simulations with initial linear fluctuations having this spectral index show that the nonlinear dark-matter structures that develop—called "halos" if isolated and "subhalos" if embedded in a larger halo—are hierarchical, with every halo and subhalo having embedded within it subhalos, in a roughly self-similar fashion. These simulations also show that halos and subhalos have singular density cusps at their centers, with the density varying with radius roughly as $\rho(r) \propto r^{-1}$ [2,3].

On scales larger than those of the stellar distribution in normal galaxies—say 10 kpc or more—the predictions of ΛCDM have been amply tested, and, although neither semianalytic theory nor numerical simulations can yet match all that we observe, the correspondence between calculation and observation is now good enough to assure us that *at large scales* the ΛCDM model is essentially correct. Particularly impressive is that the power spectrum of mass fluctuations, determined at redshift $z \sim 10^3$ by observations of the cosmic microwave background, correctly produces the power spectrum of mass fluctuations at the present time, redshift $z \simeq 0$, to within a few percent even though the amplitude at $z = 0$ is some 5 orders of magnitude larger than it was at $z \sim 10^3$.

On the other hand, on scales similar to those of galaxies, $\lesssim$10 kpc, the CDM model has essentially not been tested. In fact, the naïve predictions of the distribution of dark matter on these scales are in most cases *inconsistent* with observations [4]. As one example, the number density of galaxies varies with their total stellar mass roughly as $dn(M_\star) \propto M_*^{-1.2} dM_*$, but the predicted number density of halos increases with decreasing halo mass much more steeply, $dn(M_h) \propto M_h^{-2} dM_h$. This apparent discrepancy is usually attributed to "baryonic physics" that causes the efficiency of transforming baryons into stars to be lower in systems of lower mass. Consequently thousands of optically invisible low-mass halos ($M_h \lesssim 10^{8.5}\ M_\odot$) are predicted to exist in our Galaxy and others. A second example is the "too big to fail" problem: the high-luminosity satellite galaxies associated with the most massive subhalos appear to be much less common than CDM would predict. A third issue is that the expected dark-matter density cusps in the centers of galaxies have not been detected; this discrepancy is usually attributed to gravitational stirring of the central regions of galaxies consequent to supernova explosions, but in systems having a low baryonic fraction that explanation is problematic. Thus the hierarchical nature of density fluctuations predicted by CDM is amply established at large scales such as clusters of galaxies but—to date—the expected distribution of subhalos within the Milky Way and other galaxies has evaded detection. Given the complexity of the physics, these discrepancies are not crippling blows to the CDM model, but it can also be said that none of the characteristic features associated with CDM on galaxy scales has ever been detected.

A variant to CDM is warm dark matter (WDM), in which the mass of the hypothetical dark-matter particle is sufficiently small that its thermal velocity dispersion has a significant influence on structure formation [5]. The linear power spectrum in WDM is greatly reduced below the free-streaming scale, suppressing the formation of low-mass halos or subhalos [6,7]. The finite phase-space density prevents the development of density cusps [8], though the implied central core size is generally small [6,7].

An alternative hypothesis is that the dark matter is comprised of very light bosons or axions, $m \sim 10^{-22}$–10^{-21} eV [9–16]. All large-scale predictions are the same as in ΛCDM, but the particles' large de Broglie wavelength [Eq. (18)] suppresses small-scale structure. This material is sometimes termed "wave dark matter" or "fuzzy dark matter" (FDM), a term introduced in a seminal paper by Hu *et al.* [12]. A review of axion cosmology is given by Marsh [17]. Constraints on FDM from the cosmic microwave background are described in [18]. An attractive feature of FDM with a mass in this range is that a cosmic abundance $\Omega_m \sim 1$ can arise in naturally occurring models, as we describe below. FDM, by virtue of its macroscopic de Broglie wavelength, possesses novel features in its nonlinear dynamics. In this paper we assess the FDM hypothesis, we provide some new calculations of the properties of FDM, and we propose a set of tests to ascertain its consistency with observations. Both WDM and FDM, because they share a suppression of the power spectrum at small scales, are subject to strong constraints from the Lyman-α forest [19], which we also discuss below.

We note that all of the published (to date negative) experimental searches for dark matter and its decay products would not have detected the very light bosons that we are proposing for the principal component of the dark matter, although experiments have been suggested which have the potential to detect FDM (see discussion at the end of Sec. II A).

In Sec. II we review the physical motivation for the FDM hypothesis; in Secs. III, IV, and V we outline the astrophysical consequences, tests and predictions of the model; and in Sec. VI we summarize our conclusions. Technical calculations are relegated to several appendixes. Natural units, where $\hbar = c = 1$, are used in Sec. II A, while factors of $\hbar$ and so on are kept explicit in the rest of the paper—the

only exception is that we use eV instead of eV/c^2 to denote mass throughout.

II. THE PHYSICS OF FDM

A. Light fields of spin zero

The basic reason why it is natural in particle physics to have a very light field of spin zero is that when the mass and self-couplings of a spinless field ϕ are precisely zero, there is an extra symmetry. Thus the action

$$I = \frac{1}{2}\int d^4x\sqrt{-g}g^{\mu\nu}\partial_\mu\phi\partial_\nu\phi \tag{1}$$

has the shift symmetry $\phi \to \phi + C$, with constant C. This symmetry is lost if a mass term $\frac{1}{2}m^2\phi^2$ or a more general self-coupling $V(\phi)$ is added to the action, and likewise it could be violated by the couplings of ϕ to other fields.

The candidate particle for FDM is not a precisely massless boson, but one that is very nearly massless. Thus ϕ must have an approximate shift symmetry, not an exact one. In fact, it is suspected that in quantum gravity all continuous global symmetries, such as the shift symmetry of a scalar field, are only approximate.[1]; So we expect the symmetry to be broken at some level.

There is at least one situation in which a very light spin-zero field arises naturally: if the field ϕ is an angular variable then the potential function $V(\phi)$ must be a periodic function of ϕ. Such periodic spin-zero fields often arise in naturally occurring models, by which we mean models that were not invented for the purpose of having approximate shift symmetries. Moreover, it then often turns out that the shift symmetries are violated only by an exponentially small amount. These fields are sometimes called "axionlike fields" and the corresponding particles are likewise called "axionlike particles" because one of them could be a candidate for the QCD axion.

An axionlike candidate for FDM can be largely described by a simple model with two parameters[2] μ and F:

$$I = \int d^4x\sqrt{-g}\left[\frac{1}{2}F^2g^{\mu\nu}\partial_\mu a\partial_\nu a - \mu^4(1-\cos a)\right]. \tag{2}$$

Here a is a dimensionless scalar field with a shift symmetry $a \to a + 2\pi$. Since a is dimensionless, its kinetic energy involves the constant F (sometimes called the axion decay constant, but this terminology is misleading in the context of FDM). The periodicity $a \cong a + 2\pi$ would allow us to add to the action terms involving higher harmonics of a ($\cos ka$ or $\sin ka$ with integer k and $|k| > 1$), but in models in which μ is small enough to be relevant for our applications, those higher harmonics would have completely negligible coefficients. The mass of a is

$$m = \frac{\mu^2}{F}, \tag{3}$$

and for FDM we want $m \sim 10^{-22}$–10^{-21} eV.

For example, all models of particle physics derived from string theory have at least several periodic scalar fields such as a, and typical models have many of them (dozens or even hundreds). Various possible applications of these fields have been considered (see for example [23]). With different assumptions about their masses, they have been proposed as candidates for the inflaton field of inflationary cosmology; as potential QCD axions, whose existence may explain CP conservation by nuclear forces; and as contributors to dark energy or the cosmological constant and/or ingredients in a mechanism to explain its smallness. For our present purposes, we are interested in these fields as candidates for FDM.

In most classes of model, F lies within a relatively narrow range bounded above by the reduced Planck mass $M_{\mathrm{Pl}} = 1/\sqrt{8\pi G} = 2.435 \times 10^{18}$ GeV, and below by the traditional "grand unified" scale of particle physics, $M_G \sim 1.1 \times 10^{16}$ GeV:

$$10^{18}\ \mathrm{GeV} \gtrsim F \gtrsim 10^{16}\ \mathrm{GeV}. \tag{4}$$

The lower bound is the actual value for the "model-independent" axion of the weakly coupled heterotic string [24]. For applications to inflation, some authors have attempted to increase F beyond the upper bound of $\sim 10^{18}$ GeV, but this has proved difficult [25], except in models in which μ is so large that the axion is not relevant. The lower bound, which causes difficulty for some approaches to the QCD axion, is less firm but is valid in many classes of models [26]. As we shall see, for applications to FDM it is satisfactory to take the range (4) at face value.

What about the second parameter μ in the action? This is generated by nonperturbative instanton effects of one kind or another, depending on the model. A rough formula is

$$\mu^4 \sim M_{\mathrm{Pl}}^2\Lambda^2 e^{-S}, \tag{5}$$

[1]As a prototype of this phenomenon, for many years it appeared that the three separate lepton numbers L_e, L_μ, and L_τ were conserved quantities in particle physics. We now know from observations of neutrino oscillations that at least the separate lepton numbers $L_e - L_\mu$ and $L_\mu - L_\tau$ are violated at a very low level.

[2]The assumptions that lead to a model of this form also greatly suppress the coupling of the axion to ordinary matter. Both for this reason and because it is so light, the FDM particle would not be detected in the usual searches for WIMP dark matter or even in QCD axion searches [20–22].

where S is the instanton action and Λ, which measures a possible suppression of instanton effects due to supersymmetry, can vary over a very wide range:

$$10^{18}\ \text{GeV} \gtrsim \Lambda \gtrsim 10^{4}\ \text{GeV}. \tag{6}$$

Typical values are $\Lambda \sim 10^{18}$ GeV (no suppression due to supersymmetry), $\Lambda \sim 10^{11}$ GeV (gravity-mediated supersymmetry breaking), and $\Lambda \sim 10^{4}$ GeV (gauge-mediated supersymmetry breaking). The formula (5) is only a very rough one, but it is good enough to give an idea of how large S must be so that $m = \mu^2/F$ will be close to 10^{-22} eV. Setting $F = 10^{17}$ GeV [a different value in the range (4) would make little difference, given the uncertainties], we find that to get $m = 10^{-22}$ eV, we need

$$S = \begin{cases} 165 & \text{if } \Lambda = 10^{4}\ \text{GeV} \\ 198 & \text{if } \Lambda = 10^{11}\ \text{GeV} \\ 230 & \text{if } \Lambda = 10^{18}\ \text{GeV} \end{cases}. \tag{7}$$

The value of S is rather model dependent. In some simple cases, one finds $S \sim S_0 = 2\pi/\alpha_G$ where α_G is the Standard Model gauge coupling extrapolated to energy $M_G \sim 1.1 \times 10^{16}$ GeV. In many classes of model, S can be close to S_0 but not significantly bigger [26]. The value of α_G depends on the assumed spectrum of elementary particles up to the unification scale. The usual estimate based on known particles only gives $\alpha_G \sim 1/25$, but for example the model in [27] has $\alpha_G \sim 1/30$. Some values of S_0 are

$$S_0 = \begin{cases} 126 & \text{for } \alpha_G = 1/20 \\ 157 & \text{for } \alpha_G = 1/25 \\ 188 & \text{for } \alpha_G = 1/30 \end{cases}. \tag{8}$$

Thus the range of S_0 overlaps the desired range for S.

These numbers should not be taken very seriously, even if the basic ideas are all correct, because $2\pi/\alpha_G$ is only a very rough value for S. The reason for writing them was only to show that a mass of 10^{-22} eV is reasonable. In models with dozens or hundreds of axion-like fields, it may readily happen that the largest values of S are of order $2\pi/\alpha_G$, but that most of the axions have much smaller values of S. The axions with $S \ll 2\pi/\alpha_G$ are not candidates for FDM. In [28] (a paper that was motivated by applications to quintessence and dark energy), it is estimated that it is difficult to make S much larger than 200–300, but there is ample uncertainty in this upper bound.

To estimate what value of F will work well for FDM, we follow classic reasoning [29–31] that was originally developed to estimate the contribution to dark matter of a QCD axion. Analogous estimates for FDM have been made by several authors [23,32]. (The case of FDM is simpler as, in a minimal model of this type,[3] one does not have to estimate the turning on of strong coupling effects such as those of QCD.) One assumes that in the very early Universe, the a field was a constant with some random initial value. The logic in assuming a random initial value is this. Instead of taking the axion potential in Eq. (2) to be $\mu^4(1-\cos a)$, we could just have well have assumed $\mu^4[1-\cos(a-a_0)]$ with some constant a_0. The correct value of a_0 depends on details of the mechanism that breaks the shift symmetry at low energies. In writing Eq. (2), we shifted the field a to set $a_0 = 0$, but whatever mechanism determines the value of a in the early Universe has no way to "know" what value of a will minimize the potential at low energies.

Starting with a random initial value of a, one determines its behavior in an expanding Friedmann-Robertson-Walker (FRW) universe with metric $ds^2 = dt^2 - R(t)^2 d\mathbf{x}^2$ by simply solving the classical equation of motion for a field that depends on time only. This equation is

$$\ddot{a} + 3H\dot{a} + m^2 \sin a = 0, \tag{9}$$

with $H = \dot{R}/R$ the Hubble constant. An approximation to the behavior of this equation is that a is constant as long as $H \gtrsim m$, and then oscillates with angular frequency m (or $mc^2/\hbar$, if one restores $\hbar$ and c). The oscillations are damped as $R^{-3/2}$. In the period in which a is oscillating, it can be interpreted as describing a Bose condensate of ultralight particles of zero spatial momentum. The energy density of these particles scales as $1/R^3$, like any other form of cold dark matter. Indeed, the axion "condensate," which is just a fancy way to speak of the classical axion field, behaves for many purposes as an exceptionally cold form of CDM.

The temperature T_0 at which $H \sim m$ satisfies roughly

$$\frac{T_0^2}{M_{\rm Pl}} = m. \tag{10}$$

At that temperature, the total energy density of radiation is roughly T_0^4 and the dark-matter density [with $a \sim 1$ in Eq. (2)] is of order μ^4. As the Universe expands, the ratio of dark matter to radiation grows as $1/T$, and in the real world, they are supposed to become equal at the

[3] In a model in which, beyond well-established physics, only one field a is added, the $\mu^4 \cos a$ interaction can be understood as some sort of instanton effect (as described above), and in discussing the cosmic evolution, both F and μ can be treated as constant parameters. It is also possible to make a more complicated model with, for example, a new gauge force that becomes strong at an energy of order μ, generating the $\mu^4 \cos a$ term. Then, as in the case of the QCD axion, at temperature $T > \mu$, the $\mu^4 \cos a$ must be replaced by $(\mu/T)^n \mu^4 \cos a$, where n is a model-dependent constant.

temperature $T_1 \sim 1$ eV at which the Universe becomes matter dominated. So we want

$$\frac{\mu^4}{T_0^4}\frac{T_0}{T_1} \sim 1. \tag{11}$$

Combining these formulas and using $\mu^4 = F^2 m^2$, we get

$$F \sim \frac{M_{\rm Pl}^{3/4} T_1^{1/2}}{m^{1/4}} \sim 0.5 \times 10^{17}\ \text{GeV}, \tag{12}$$

for $m \sim 10^{-22}$ eV. The fact that this is in the range described earlier in Eq. (4) is an interesting coincidence, somewhat reminiscent of the weakly interacting massive particle (WIMP) miracle. In other words, the axion energy density today (normalized by the critical density) is

$$\Omega_{\rm axion} \sim 0.1\left(\frac{F}{10^{17}\ \text{GeV}}\right)^2\left(\frac{m}{10^{-22}\ \text{eV}}\right)^{1/2}. \tag{13}$$

The temperature T_0 at which the FDM field begins to oscillate is

$$T_0 \sim (m M_{\rm Pl})^{1/2} \sim 500\ \text{eV}. \tag{14}$$

This corresponds to a redshift $\sim 2 \times 10^6$. This is after nucleosynthesis, so FDM behaves during nucleosynthesis as a (negligible) contribution to dark energy.

In the axion model, is the dynamics of dark matter purely gravitational or do we have to consider the axion self-interaction? In the two-parameter model of Eq. (2), once $F \sim 10^{17}$ GeV and $m \sim 10^{-22}$ eV are determined from observed properties of dark matter, the coefficients of the nonlinear axion interactions are determined. Thus the axion equation of motion, including terms of cubic order in a, is

$$0 = D_\mu D^\mu a + m^2 a - \frac{m^2}{6}a^3 + \mathcal{O}(a^5). \tag{15}$$

To decide whether the a^3 term, which is attractive, is significant, we can proceed as follows. In a body with a dimensionless gravitational potential ε, the gravitational contribution to the equation is of order $\varepsilon m^2 a$. The condition for the a^3 term to be significant in comparison to gravity is therefore $m^2 a^3 \gtrsim \varepsilon m^2 a$ or $a^2 \gtrsim \varepsilon$. We will evaluate this condition in the very early Universe and in today's Universe.

At the temperature T_0 at which dark matter begins to oscillate dynamically, we have $a^2 \sim 1$ (since we have assumed a random initial value of a) and $\varepsilon \sim 10^{-5}$ (the value of the primordial cosmic fluctuations). Thus $a^2 \gg \varepsilon$ and the self-interaction of a dominates. This continues until a diminishes by a factor of about $10^{-5/2}$. Since $a \sim R^{-3/2}$, gravity dominates once R increases by a factor of about $10^{5/3}$. Thus gravity dominates below a temperature of roughly $10^{-5/3}T_0$, and in particular gravity dominates by the time the temperature T_1 of radiation-matter equality is reached.

On the other hand, for a weakly bound object of density ρ and size L in today's Universe, we have $\varepsilon \sim G\rho L^2$. As the dark-matter density is $\rho \sim F^2 m^2 a^2$, the condition $a^2 \gtrsim \varepsilon$ for the nongravitational force to be significant is $1 \gtrsim GF^2 m^2 L^2$ or

$$L \lesssim \frac{\sqrt{8\pi} M_P}{Fm}. \tag{16}$$

Quantitatively, for $F \sim 10^{17}$ GeV, $m \sim 10^{-22}$ eV, this says that gravity dominates for a dark-matter-dominated object of size greater than roughly 1 parsec.

What are the difficulties with the axion approach to FDM? We will just mention a couple of the more obvious issues. One question is what to make of axionlike particles other than the one that hypothetically makes up FDM. Axions with a larger value of S (and therefore a smaller mass) than the FDM particle are really not a problem. They simply make small contributions to the dark matter or the dark energy in today's Universe.[4] Axions with a mass larger than about 10^4 GeV (which corresponds to $S \sim 50$ if, for example, $\Lambda \sim 10^{11}$ GeV) may decay quickly enough to cause no cosmological difficulties. However, axionlike particles with masses in the large range $10^4\ \text{GeV} \gtrsim m \gtrsim 10^{-22}$ eV could potentially create too much dark matter. An optimist might hope that the world is described by a model in which there are no axions with (roughly) $50 < S < 200$. Another issue concerns the tensor-to-scalar ratio r of cosmological perturbations. In a model in which r is large enough to be observed, under the simplest assumptions a QCD axion in the range $F \gtrsim 10^{16}$ GeV that is assumed in the above discussion leads to isocurvature fluctuations that are excluded by cosmological observations. (For an assessment, see for example [33]. The problem arises because the same mechanism that leads to quantum fluctuations of order $H/2\pi$ for the inflaton field leads to fluctuations of the same order for any sufficiently light axion field. Independent fluctuations in two different scalar fields lead to isocurvature perturbations.) There is an analogous although less severe problem for a FDM particle. The problem is less severe because the parameters of this particle have been adjusted so that the maximum dark

[4]Axionlike fields that are oscillating in today's Universe represent contributions to dark matter. Those with masses less than today's Hubble constant are still not oscillating in the present Universe and represent contributions to the dark energy. It is argued in [28] that axion contributions are too small to account for all of the dark energy except possibly in a situation with a very large number of axions contributing. (In any event, we stress that an axion in the mass range appropriate to FDM definitely behaves as a contribution to dark matter, not dark energy.)

matter it can produce is comparable to what is observed (by contrast a QCD axion with $F \gtrsim 10^{16}$ GeV is at risk of producing much too much dark matter). But there still is a potential difficulty, if r is observed. We will have to wait to see if this is a problem that needs to be solved.

If FDM exists, can it be detected in any way other than by observing its gravitational effects? Conventional dark matter searches would not find the FDM particle both because it is much too light and because it couples much too weakly to ordinary matter (if it had strong nongravitational couplings to ordinary matter, then allowing for quantum effects, it would not be as light as described above).[5] However, a number of proposals for direct, or at least more direct, observation of ultralight axionlike particles have been made in [23]. The value $m \sim 10^{-22}$–10^{-21} eV is not optimal for most of these proposals, but is at the edge of what might be detected by observing certain effects involving supermassive black holes. It has been suggested (in [32] and by P. Graham, private communication) that the CASPEr-Wind version of the CASPEr axion experiment might ultimately have the sensitivity to observe FDM. This experiment is described, though not by that name, in Sec. 5 A of [34]. FDM might also be eventually detectable less directly by pulsar timing observations [35].

B. FDM as a superfluid

From the above discussion, we see that for the purpose of studying structures on galactic scales and above, we can ignore the self-interaction of the axionlike particle. In other words, let us consider the following action for a scalar[6] ϕ, minimally coupled to the metric $g_{\mu\nu}$:

$$S = \int \frac{d^4x}{\hbar c^2}\sqrt{-g}\left[\frac{1}{2}g^{\mu\nu}\partial_\mu\phi\partial_\nu\phi - \frac{1}{2}\frac{m^2c^2}{\hbar^2}\phi^2\right], \quad (17)$$

where we have restored factors of c and $\hbar$, with ϕ having energy units. We are interested in a mass m that corresponds to an astronomically relevant de Broglie wavelength:

$$\frac{\lambda}{2\pi} = \frac{\hbar}{mv} = 1.92\ \mathrm{kpc}\left(\frac{10^{-22}\ \mathrm{eV}}{m}\right)\left(\frac{10\ \mathrm{km\,s^{-1}}}{v}\right) \quad (18)$$

where v is the velocity. A collection of a large number of such particles in the same state can be described by a classical scalar field. In the nonrelativistic limit, it is helpful to express ϕ in terms of a complex scalar ψ:

$$\phi = \sqrt{\frac{\hbar^3 c}{2m}}(\psi e^{-imc^2t/\hbar} + \psi^* e^{imc^2t/\hbar}). \quad (19)$$

As is well known, the equation of motion for ψ takes the form of the Schrödinger equation, assuming $|\ddot{\psi}| \ll mc^2|\dot{\psi}|/\hbar$:

$$i\hbar\left(\dot{\psi} + \frac{3}{2}H\psi\right) = \left(-\frac{\hbar^2}{2mR^2}\nabla^2 + m\Phi\right)\psi, \quad (20)$$

where $\Phi(\mathbf{r}, t)$ is the gravitational potential and we have adopted the perturbed FRW metric,

$$ds^2 = \left(1 + \frac{2\Phi}{c^2}\right)c^2dt^2 - R^2(t)\left(1 - \frac{2\Phi}{c^2}\right)d\mathbf{r}^2. \quad (21)$$

For many Galactic dynamics applications it is sufficient to set the scale factor $R(t)$ to unity, and the Hubble parameter $H \equiv \dot{R}/R$ to zero. The scalar ψ should be interpreted as a classical field, quantum fluctuations around which are small. The situation is analogous to using the Maxwell equations to describe configurations involving a large number of photons (see [36] for a discussion; see also [37,38] for the use of the Schrödinger equation in modeling large-scale structure).

It is sometimes useful to think of the dark matter as a fluid, a superfluid in fact. We define the fluid density ρ and velocity $\mathbf{v}$ by

$$\psi \equiv \sqrt{\frac{\rho}{m}}e^{i\theta}, \quad \mathbf{v} \equiv \frac{\hbar}{Rm}\nabla\theta = \frac{\hbar}{2miR}\left(\frac{1}{\psi}\nabla\psi - \frac{1}{\psi^*}\nabla\psi^*\right). \quad (22)$$

The vorticity of the flow $\nabla \times \mathbf{v}$ vanishes, though the more physically relevant quantity is the momentum density which has nonzero curl in general. The following equations can be derived from the ψ equation of motion in comoving coordinates:

$$\dot{\rho} + 3H\rho + \frac{1}{R}\boldsymbol{\nabla}\cdot(\rho\mathbf{v}) = 0, \quad (23)$$

$$\dot{\mathbf{v}} + H\mathbf{v} + \frac{1}{R}(\mathbf{v}\cdot\boldsymbol{\nabla})\mathbf{v} = -\frac{1}{R}\boldsymbol{\nabla}\Phi + \frac{\hbar^2}{2R^3m^2}\boldsymbol{\nabla}\left(\frac{\nabla^2\sqrt{\rho}}{\sqrt{\rho}}\right). \quad (24)$$

These are known as the Madelung equations, slightly generalized to an expanding universe (see the Feynman lectures [39] for a discussion, and also [40–44]). They strongly resemble the continuity and Euler equations of classical fluid mechanics with the addition of the second term on the right of Eq. (24), commonly referred to as the "quantum pressure" term. The quantum pressure gives rise

[5] A derivative coupling of the axion to fermions is allowed, as is a coupling $a\epsilon^{\mu\nu\alpha\beta}f_{\mu\nu}f_{\alpha\beta}$ where $f_{\mu\nu}$ is the electromagnetic field strength. Such couplings will be proportional to $1/F$ in the sort of model assumed above, which drastically suppresses their effects.

[6] We use a canonically normalized scalar field ϕ, related to the dimensionless field a used in the last subsection by $\phi = Fa$.

to a certain "stiffness" of the FDM fluid that resists compression.

More precisely, the quantum pressure arises from a stress tensor $\boldsymbol{\sigma}$,

$$\dot{\mathbf{v}} + H\mathbf{v} + \frac{1}{R}(\mathbf{v}\cdot\boldsymbol{\nabla})\mathbf{v} = -\frac{1}{R}\boldsymbol{\nabla}\Phi + \frac{1}{R}\boldsymbol{\nabla}\cdot\boldsymbol{\sigma}, \quad (25)$$

where

$$\sigma_{ij} = -\frac{\hbar^2}{4m^2R^2}\left(\frac{1}{\rho}\frac{\partial\rho}{\partial x_i}\frac{\partial\rho}{\partial x_j} - \frac{\partial^2\rho}{\partial x_i\partial x_j}\right) = \frac{\hbar^2\rho}{4R^2m^2}\frac{\partial^2\log\rho}{\partial x_i\partial x_j}. \quad (26)$$

An equivalent form is

$$\partial_t(\rho v_i) + 4H\rho v_i + \frac{1}{R}\partial_j\Pi_{ij} + \frac{1}{R}\rho\partial_i\Phi = 0 \quad (27)$$

where the momentum flux density tensor is

$$\Pi_{ij} = \rho v_i v_j - \sigma_{ij} = \frac{\hbar^2}{4mR^2}(\partial_i\psi^*\partial_j\psi + \partial_i\psi\partial_j\psi^* - \psi^*\partial_i\partial_j\psi - \psi\partial_i\partial_j\psi^*) \quad (28)$$

up to the addition of a divergence-free tensor.

The Madelung equations are well suited to numerical simulations, because standard hydrodynamics codes can be modified to incorporate the quantum pressure [16,45,46]. As an example of the relation between the fluid and scalar field viewpoints, a discussion of the collision of streams is given in Appendix E.

To minimize confusion, we would like to point out that despite the appearance of $\hbar$ in many of the above formulas, all of the considerations above and in this paper can be understood purely in terms of classical field theory. Indeed, $\hbar$ and the mass m appear only in the form of the ratio $\hbar/m$. All of our formulas can be expressed in terms of this ratio without ever mentioning $\hbar$.

III. ASTROPHYSICS OF FDM IN THE MILKY WAY AND NEARBY GALAXIES

A. Introductory remarks

The differences between the properties of a standard CDM Universe and a Universe in which the dark matter is dominated by FDM will be most prominent in dark-matter-dominated systems where the de Broglie wavelength $\lambda = h/(mv)$ is comparable to the system size r. Since the virial velocity v of halos or subhalos generally decreases as r decreases this condition favors small systems, both because r is small and because λ is large. Given the small scales, the effects of FDM are most easily studied in nearby systems, so most of the tests described below are best performed in the Milky Way or other Local Group galaxies. On the other hand, in the standard ΛCDM model of structure formation, small-scale systems form earliest, so the differences between galaxy formation in CDM- and FDM-dominated universes will be most dramatic at high redshift. Thus the very near, in this section, and the very far, in Secs. IV and V, will be the foci of our attention.

B. Minimum size and maximum density

The de Broglie wavelength for FDM is given by Eq. (18). Roughly speaking, $\lambda/(2\pi)$ cannot exceed the virial radius $r \simeq GM/v^2$ of an equilibrium self-gravitating system of mass M. Thus $r \gtrsim \hbar^2/(GMm^2)$. A more precise statement, derived in Appendix B, is that the radius containing half the mass of a spherically symmetric, time-independent, self-gravitating system of FDM must satisfy the inequality

$$r_{1/2} \geq 3.925\frac{\hbar^2}{GMm^2} = 0.335\ \mathrm{kpc}\frac{10^9\ M_\odot}{M}\left(\frac{10^{-22}\ \mathrm{eV}}{m}\right)^2. \quad (29)$$

The inequality is an equality if the system is in a stationary state that minimizes the energy[7] this state is sometimes called a "soliton." Similarly, the central density satisfies

$$\rho_c \leq 0.0044\left(\frac{Gm^2}{\hbar^2}\right)^3 M^4 = 7.05\ M_\odot\,\mathrm{pc}^{-3}\left(\frac{m}{10^{-22}\ \mathrm{eV}}\right)^6\left(\frac{M}{10^9\ M_\odot}\right)^4. \quad (30)$$

This upper limit to the density can be compared with the observed central densities of dwarf spheroidal galaxies in the Local Group, which are strongly dominated by dark matter even at their centers: many have mass-to-light ratios $\gtrsim 100\ M_\odot/L_\odot$ inside their half-light radii. Among 36 Local Group dwarf spheroidals the maximum, mean and median density within the half-light radius are 5, 0.5, and 0.1 $M_\odot\mathrm{pc}^{-3}$ [48], consistent with Eq. (30) if $m \simeq 10^{-22}$ eV and the ground-state mass exceeds $3\times10^8\ M_\odot$–$10^9\ M_\odot$. With these nominal values the halo half-mass radius (29) is similar to the observed half-light radii of dwarf spheroidal galaxies: the median and quartiles for the Local Group sample are $0.25^{+0.3}_{-0.1}$ kpc.

If we assume that the central part of the halo is a soliton it is possible to fit the kinematics of the stars in dwarf spheroidal galaxies to determine the FDM particle mass.

[7] In the approximation of the Schrödinger-Poisson equation there is a conserved particle number, and the soliton solution minimizes the energy for a given particle number. This particle number is not conserved in the full equations governing a real scalar field interacting with gravity, so in that context the soliton is not absolutely stable, although its lifetime is much greater than the Hubble time [47].

Using eight dwarf spheroidals, Chen *et al.* [49] found masses between $m = 8^{+5}_{-3} \times 10^{-23}$ eV (for Draco) and $m = 6^{+7}_{-2} \times 10^{-22}$ eV (for Sextans). The galaxy-to-galaxy scatter in m can be ascribed to contamination by foreground stars, the strong covariance between the observational determination of the central density ρ_c and the half-mass radius $r_{1/2}$, and perhaps the assumption that the central part of the halo is a soliton. Other estimates, based on fewer galaxies or more approximate models, are roughly consistent [16,50,51].[8]

C. Relaxation in systems composed of FDM

Over distances that are large compared to the de Broglie wavelength, FDM behaves similarly to CDM. Thus we expect the soliton to be surrounded by a virialized halo with a Navarro-Frenk-White (NFW) profile [3]. This expectation is demonstrated by simulations [16,45,53,54]. Simulations yield a relation between the mass of the central soliton M and the virial mass of the surrounding halo $M_{\rm vir}$ [53],

$$M \simeq 2.7 \times 10^8\ M_\odot \frac{10^{-22}\ \text{eV}}{m} \left(\frac{M_{\rm vir}}{10^{10}\ M_\odot}\right)^{1/3}; \qquad (31)$$

however, this relation has only been well tested over the limited range $10^9\ M_\odot \lesssim M_{\rm vir} \lesssim 10^{11}\ M_\odot$. These simulations show up to 2 orders of magnitude difference in density between the solitonic core and the surrounding halo. At larger halo masses the density contrast between the solitonic core and the halo is expected to be even larger, but the soliton mass should fall below the estimate from Eq. (31), for reasons given below.

An isolated CDM system that is in equilibrium (i.e., that satisfies the time-independent collisionless Boltzmann equation) evolves only through two-body relaxation [55], on a time scale of order $t_{\rm relax} \sim 0.1 t_{\rm cr}(M/m)$ where $t_{\rm cr} \sim r/v$ is the crossing time and we have neglected a logarithmic factor. For typical galaxy masses M and CDM particle masses $m_{\rm CDM}$, $t_{\rm relax}$ is many orders of magnitude longer than the Hubble time. In contrast, a FDM system that is not a soliton evolves by expelling probability density to infinity since all eigenstates other than the solitonic ground state are unstable. This process is sometimes called "gravitational cooling" [45,56–58], and the wavy granularity that is the source of this relaxation is seen clearly in simulations [16]. The granularity, which can also be thought of as an interference pattern, arises from two distinct sources: the finite number of modes or eigenstates in the halo—of order $(kr)^3$ where $2\pi/k = \lambda \sim h/(mv)$ is the de Broglie wavelength—and the spatial correlation in density fluctuations that arises because the FDM particles are bosons (similar to the Hanbury-Brown and Twiss effect for photons). The strength of the fluctuations and their dynamical effect can be estimated by the following crude arguments. If the local density is ρ then the FDM acts as quasiparticles with effective mass $m_{\rm eff} \sim \rho(\frac{1}{2}\lambda)^3$. Then the relaxation time should be $t_{\rm relax} \sim 0.1 t_{\rm cr} M/m_{\rm eff}$ where $M \sim \frac{4}{3}\pi\rho r^3$ is the halo mass interior to radius r. We find[9]

$$\begin{aligned} t_{\rm relax}(r) &\sim \frac{0.4}{f_{\rm relax}} \frac{m^3 v^2 r^4}{\pi^3 \hbar^3} \\ &\sim \frac{1 \times 10^{10}\ \text{yr}}{f_{\rm relax}} \left(\frac{v}{100\ \text{km s}^{-1}}\right)^2 \\ &\quad \times \left(\frac{r}{5\ \text{kpc}}\right)^4 \left(\frac{m}{10^{-22}\ \text{eV}}\right)^3, \end{aligned} \qquad (32)$$

where $f_{\rm relax} \lesssim 1$ is a dimensionless constant, the value of which remains to be estimated by simulations and/or more careful analytic arguments.

A FDM halo will develop a compact solitonic core from the mass originally in the halo inside radius r_s, where r_s is given approximately by the condition $t_{\rm relax}(r_s) = t_0$ and t_0 is the age of the halo. Low-mass halos have relatively small radii and virial velocities so the relaxation time is short and most of the halo is incorporated in the soliton. As the halo mass grows the virial radius and virial velocity increase, $r_{\rm vir} \sim M_{\rm vir}^{1/3}$ and $v_{\rm vir} \sim M_{\rm vir}^{2/3}$, so the relaxation time grows and only a small fraction of the halo mass resides in the central soliton. The soliton mass depends on the density and velocity distribution in the halo, which is approximately described by a NFW profile [3]. Thus the simple relation (31) between the virial mass and the soliton mass is probably an approximation that is only valid over a limited range of virial masses. The NFW density profile flattens at small radii so we expect the curve relating soliton mass to virial mass to flatten, and possibly even have negative slope, at large virial masses.

The fluctuating gravitational potential whose effects are described by Eq. (32) also leads to relaxation in the stellar components of the galaxy, although possibly with a different dimensionless constant. Some of the relevant dynamics has already been described in the context of dark matter composed of massive black holes [59] or dark clusters [60]. To make a rough estimate of the importance of this process, we focus on the Milky Way at the distance of the Sun, taking $r \sim 10$ kpc, $v \sim 200\ \text{km s}^{-1}$, $\rho \sim 0.01\ M_\odot\ \text{pc}^{-3}$. Then the de Broglie wavelength $\lambda \simeq 600\ \text{pc}(10^{-22}\ \text{eV}/m)$ and the mass of a typical quasiparticle is $m_{\rm eff} \sim \rho(\frac{1}{2}\lambda)^3 \sim 3 \times 10^5\ M_\odot (10^{-22}\ \text{eV}/m)^3$. The possible effects include.

[8] An exception is the recent paper by Gonzáles-Morales *et al.* [52], which finds $m < 0.4 \times 10^{-22}$ eV from analyzing the kinematics of stars in the Fornax and Sculptor dwarf galaxies.

[9] Thus FDM has less bound substructure than CDM but more unbound substructure.

1. Disruption of star clusters

The fluctuating potential from FDM wave packets exerts tidal forces that can pump energy into open and globular clusters. The disruption time can be estimated from Eq. (8.54) of [55],

$$t_{\rm dis} \simeq \frac{0.05}{f_{\rm relax}} \frac{\sigma_{\rm rel} m_{\rm cl} r_h^2}{G m_{\rm eff} \rho a^3}. \tag{33}$$

Here $\sigma_{\rm rel} \sim v$ is the one-dimensional dispersion in relative velocity; $m_{\rm cl}$ is the cluster mass; r_h is the half-mass radius of the perturber, which we take to be $\frac{1}{2}\lambda$; and a is the radius or semimajor axis of the cluster star relative to the cluster center. This formula assumes that $r_h \gg a$, that the maximum velocity kick from a passing FDM quasiparticle is much less than the escape speed from the cluster, and that the passage time of the quasiparticle r_h/v is shorter than the dynamical time in the cluster; all of these assumptions are reasonable for the examples discussed here. Inserting nominal parameters for globular clusters,

$$t_{\rm dis} = \frac{8.4\times10^{11}\ {\rm yr}}{f_{\rm relax}} \left(\frac{v}{200\ {\rm km\,s^{-1}}}\right)^2 \left(\frac{m_{\rm cl}}{3\times10^5\ M_\odot}\right) \times \left(\frac{m}{10^{-22}\ {\rm eV}}\right) \left(\frac{0.01\ M_\odot\,{\rm pc^{-3}}}{\rho}\right)^2 \left(\frac{30\ {\rm pc}}{a}\right)^3. \tag{34}$$

For the nominal parameters the disruption time is much too large to be of interest. However, the disruption time is shorter at smaller distances from the Galactic center because the FDM density ρ is much larger and $t_{\rm dis} \sim \rho^{-2}$. Thus globular clusters close to the Galactic center could be shorn of their outer parts or even disrupted by FDM fluctuations if $f_{\rm relax} \sim 1$. The outer parts of one or two of the globular clusters in the Fornax dwarf galaxy could also be susceptible to disruption by this process.[10] Open clusters have a wide range of masses, radii, and ages but for the nominal values $m_{\rm cl} = 300\ M_\odot$ and $a = 2$ pc we find $t_{\rm dis} \simeq 2\times10^{11}\ {\rm yr}/f_{\rm relax}$ compared to a typical age of 3×10^8 yr; we conclude that for open clusters in the solar neighborhood the effects of FDM fluctuations are negligible.

2. Disruption of wide binary stars

The effect of FDM fluctuations on binary stars can be described by Eq. (34) if we replace the cluster mass $m_{\rm cl}$ by the total mass of the binary, which we take to be $2\ M_\odot$, and let a represent the binary semimajor axis. The widest known binary stars have $a \simeq 0.1$ pc so we obtain $t_{\rm dis} \simeq 1.5\times10^{14}\ {\rm yr}/f_{\rm relax}$, too long to be of interest.

[10]T. Brandt, private communication.

3. Thickening of the Galactic disk

FDM fluctuations can pump energy into the orbits of disk stars. An approximate estimate of the characteristic time for the disk to double in thickness is

$$t_{\rm thick} = \frac{0.2}{f_{\rm relax}} \frac{\sigma_{\rm disk}^2 v b_{\rm min}^2}{G^2 m_{\rm eff} \rho z_{1/2}^2}. \tag{35}$$

Here $\sigma_{\rm disk}$ and $z_{1/2}$ are the vertical velocity dispersion and half-thickness of the disk and $b_{\rm min}$ is the minimum impact parameter of encounters that contribute strongly to the thickening. We set $b_{\rm min} = \max(z_{1/2}, \frac{1}{2}\lambda)$. We have $\lambda > 2z_{1/2}$ for $m < 1.0\times10^{-22}\ {\rm eV}(200\ {\rm km\,s^{-1}}/v)(300\ {\rm pc}/z_{1/2})$; in this case

$$t_{\rm thick} = \frac{7.0\times10^{11}\ {\rm yr}}{f_{\rm relax}} \left(\frac{\sigma_{\rm disk}}{30\ {\rm km\,s^{-1}}}\right)^2 \left(\frac{v}{200\ {\rm km\,s^{-1}}}\right)^2 \times \left(\frac{m}{10^{-22}\ {\rm eV}}\right) \left(\frac{0.01\ M_\odot\,{\rm pc^{-3}}}{\rho}\right)^2 \left(\frac{300\ {\rm pc}}{z_{1/2}}\right)^2. \tag{36}$$

For larger masses, when $\lambda < 2z_{1/2}$,

$$t_{\rm thick} = \frac{7.0\times10^{11}\ {\rm yr}}{f_{\rm relax}} \left(\frac{\sigma_{\rm disk}}{30\ {\rm km\,s^{-1}}}\right)^2 \left(\frac{v}{200\ {\rm km\,s^{-1}}}\right)^4 \times \left(\frac{m}{10^{-22}\ {\rm eV}}\right)^3 \left(\frac{0.01\ M_\odot\,{\rm pc^{-3}}}{\rho}\right)^2. \tag{37}$$

These time scales are too long to be of interest in the solar neighborhood, but thickening by FDM fluctuations could convert disks into thicker structures such as pseudobulges in the inner parts of galaxies.

4. Galactic bulges

The bulges of disk galaxies have typical sizes of ~1 kpc and thus would interact strongly with FDM fluctuations according to Eq. (32). However, this equation probably overestimates the relaxation rate inside the region where $t_{\rm relax}$ is less than the age of the galaxy because most of the FDM will be incorporated in the central soliton, which is stationary and does not contribute to relaxation.

5. Orbital decay of supermassive black holes

Most galaxies contain black holes of $10^6\ M_\odot$–$10^{10}\ M_\odot$ at their centers. When two galaxies with CDM halos merge, dynamical friction from the halo drains orbital energy from the black holes and they spiral in to the central few parsecs of the merger remnant [61,62]. If the inspiral continues to even smaller orbital radii, until the decay time scale due to gravitational radiation becomes shorter than a Hubble time (typically at semimajor axes of 0.001–0.1 pc), then the two black holes will merge. The gravitational radiation from the

late stages of the inspiral and the merger could be detectable by ground-based pulsar timing arrays and space-based interferometers, respectively. However, FDM fluctuations may inhibit the inspiral at kiloparsec scales. The effective mass of the FDM quasiparticles $m_{\rm eff} \sim \rho_{\rm FDM}(\frac{1}{2}\lambda)^3$ can be rewritten using the relation $\rho \sim 3v^2/(4\pi G r^2)$ if ρ is interpreted as the mean density inside radius r and FDM dominates this density so $\rho \sim \rho_{\rm FDM}$. Then

$$m_{\rm eff} \sim \frac{3\pi^2\hbar^3}{4Gr^2m^3v} = 6\times 10^7\, M_\odot \left(\frac{1\ {\rm kpc}}{r}\right)^2 \left(\frac{200\ {\rm km\,s^{-1}}}{v}\right)\left(\frac{10^{-22}\ {\rm eV}}{m}\right)^3. \tag{38}$$

At small radii, but outside the solitonic core, the effective mass of the FDM fluctuations can be larger than the black-hole mass and in this case the fluctuations will pump energy into the black-hole orbits, opposing the drain of energy by dynamical friction from the hot stellar component (an additional effect in disk galaxies is dynamical friction from rotating stars and gas in the disk, which adds to the component of angular momentum normal to the disk). If the density of FDM is comparable to the density of stars and other baryons, the orbital decay could be slowed or even reversed; if the stellar system has density $\rho_\star$ and is not rotating, and the black hole has mass $m_{\rm BH}$, this reversal occurs if there is a radial region where $\rho_{\rm FDM} m_{\rm eff} \gtrsim \rho_\star m_{\rm BH}$. In this case the formation of subparsec black-hole binaries would be suppressed, and the rate of black-hole mergers could be much smaller than otherwise predicted. The predicted population of supermassive black holes orbiting at kiloparsec distances from the centers of galaxies would be extremely difficult to detect.

These speculations and estimates require confirmation by more sophisticated analytic arguments and simulations. They suggest that relaxation due to FDM fluctuations may substantially alter the structure of both the inner parts of galaxy-size FDM halos and their stellar components.

D. The cusp-core problem

A generic prediction of structure formation in CDM is that halos and subhalos should have singular density cusps at their centers, with the density varying with radius roughly as $\rho(r) \sim r^{-1}$ [2,3]. Baryonic processes such as adiabatic contraction, infalling substructure, or density fluctuations due to supernova feedback could modify this profile [63–73], so the prediction of a central density cusp is most secure in dwarf spheroidal galaxies, where the total density is strongly dominated by dark matter at all radii [48].

In principle, observations of stellar kinematics can determine whether the dark-matter density distribution at the centers of dwarf spheroidals is a cusp as in CDM models or a core as in FDM. Although the majority of studies favor cores over cusps, the question has not yet been settled, largely because of degeneracies between the observational signatures of the mass profile and the velocity anisotropy profile [74–86]. The density profiles of low-surface-brightness disk galaxies also appear to have cores [87–89]; see [90] for a review.

We conclude that the kinematics of low-surface-brightness galaxies, both dwarf spheroidals and disks, is consistent with the cores required by FDM and disfavors, but does not rule out, CDM. Definitive observations of dark-matter cusps down to a distance r from the centers of galaxies would rule out FDM with a mass $m \lesssim \hbar/(vr)$ where v is the velocity dispersion at r.

E. Lower bound on FDM halo masses

We have seen [Eq. (29)] that self-gravitating time-independent FDM systems supported by quantum pressure have the unusual property that low-mass objects are larger than those of higher mass. This has important cosmological consequences that are independent of the details of the halo formation process and the spectrum of initial density perturbations, in particular a minimum mass for FDM halos.

There are two arguments based on similar physical principles that produce the same lower bound on the halo mass. The first is based on the observation that if halos form by gravitational collapse they cannot be lower in density than the average universe in which they reside. Let $\rho_{1/2} = \frac{1}{2}M/(\frac{4}{3}\pi r_{1/2}^3)$ be the mean density inside the half-mass radius [Eq. (29)]. For comparison, the virial radius is commonly defined such that the mean density inside it is $\rho_{\rm vir} \equiv 200\rho_{\rm crit}$ where $\rho_{\rm crit} = 3H^2/(8\pi G)$ is the critical density. If we require that $\rho_{1/2} > q\rho_{\rm vir}$ where q is a factor $\gtrsim 1$ then

$$M > 2.8 q^{1/4}\frac{H^{1/2}\hbar^{3/2}}{Gm^{3/2}} = 1.4\times 10^7\, M_\odot q^{1/4}\left(\frac{H}{70\ {\rm km\,s^{-1}\ Mpc^{-1}}}\right)^{1/2} \times \left(\frac{10^{-22}\ {\rm eV}}{m}\right)^{3/2}. \tag{39}$$

The second argument is based on the Jeans length, the minimum scale for gravitationally unstable density perturbations in a homogeneous background. This has been derived for FDM and gives for the critical (maximum) Jeans wave number [12,41,42,91–94]

$$k_J = \frac{2(\pi G\rho)^{1/4}m^{1/2}}{\hbar^{1/2}} \tag{40}$$

where ρ is the unperturbed matter density and k_J is in physical, not comoving, coordinates. The corresponding Jeans length is $\lambda_J \equiv 2\pi/k_J$ and the Jeans mass is

$$M_J = \frac{4}{3}\pi\rho\left(\frac{1}{2}\lambda_J\right)^3 \tag{41}$$

$$= 1.5\times 10^7\ M_\odot (1+z)^{3/4}\left(\frac{\Omega_{\rm FDM}}{0.27}\right)^{1/4} \times \left(\frac{H_0}{70\ {\rm km\,s^{-1}\ Mpc^{-1}}}\right)^{1/2}\left(\frac{10^{-22}\ {\rm eV}}{m}\right)^{3/2}. \tag{42}$$

Here H_0 is the Hubble constant and $\Omega_{\rm FDM}$ is the fraction of the critical density in FDM. Within the considerable uncertainties Eqs. (39) and (42) give the same result, a minimum halo mass of $(1\text{–}2)\times 10^7\ M_\odot(10^{-22}\ {\rm eV}/m)^{3/2}$, in fairly good agreement with an earlier estimate by [53], $4\times 10^7\ M_\odot(10^{-22}\ {\rm eV}/m)^{3/2}$, obtained by setting $M = M_{\rm vir}$ in Eq. (31). For CDM the number of halos (and subhalos) is rising as $dn(M_h)\propto M_h^{-2}dM_h$ below $10^8\ M_\odot$, so the contrast in the number of low-mass halos is dramatic.

Dark-matter halos or subhalos cannot easily exist with masses lower than this limit, so dark-matter halos around globular clusters or similar ultracompact dwarf galaxies are not expected in FDM models [94].

Whether or not halos form at or near this minimum mass depends on the initial density perturbation spectrum for FDM and its linear and nonlinear growth, a topic we defer to Sec. IV.

F. A maximum soliton mass

At sufficiently large mass M the depth of the central potential of a solitonic core composed of FDM approaches c^2. From Eq. (B3) this occurs when $M\sim\hbar c/(Gm)$ and this represents a maximum mass for FDM solitons analogous to the Chandrasekhar mass for self-gravitating fermion systems. Calculations that employ general relativity [95–97] provide a more accurate value,

$$M_{\rm max} = 0.633\frac{\hbar c}{Gm} = 8.46\times 10^{11}\ M_\odot\frac{10^{-22}\ {\rm eV}}{m}. \tag{43}$$

FDM halos can and do exist with much larger masses. In such cases the mass of the central soliton is only a small fraction of the total halo mass, most of the halo behaves classically, and the mass spectrum and most other properties of halos would be the same as in CDM. An unresolved question is how the relaxation processes described in Sec. III C would affect the central structure in massive FDM halos. The maximum soliton mass is lowered when the self-interaction expected for an axion is taken into account [98,99].

G. The missing-satellite problem

Structure formation in standard ΛCDM cosmology is approximately self-similar, with every gravitationally bound halo containing bound subhalos "all the way down." However, the expected distribution of CDM subhalos in massive galaxies greatly exceeds the number of small satellite galaxies observed to orbit luminous galaxies [100,101]. This discrepancy is often called the "missing satellite" problem. The most commonly proposed solutions to this problem invoke baryonic physics, in particular (i) heating of the halo gas by ultraviolet background radiation, which could suppress gas accretion onto subhalos, and (ii) supernovae and stellar winds, which could drive most of the gas out of the subhalos. The conclusions to be drawn from recent examinations of these processes [102,103] are unclear. Heating and feedback certainly reduce the stellar luminosity of the satellite galaxies associated with subhalos, but whether plausible parametrizations for these processes can match the observations over the full range of halo and subhalo masses remains an open question.

The missing-satellite problem is reduced or resolved in FDM without appeal to baryonic physics, because the number of low-mass subhalos is expected to be much smaller in FDM than in CDM. There are two main reasons for this. The first is that subhalos are more vulnerable to tidal disruption, both because of the upper limit to their mass density [Eq. (30)], and because FDM can tunnel through the potential barrier centered on the tidal radius; thus a FDM subhalo is *always* disrupted by a tidal field, no matter how weak, after a sufficiently long time. A simplified model of this process for FDM solitons is described in Appendix C. We find that a FDM soliton cannot survive on a circular orbit in a host system for $\gtrsim$10 orbits[11] unless its central density $\rho_c > 60\bar{\rho}_{\rm host}$; survival for a few hundred orbits requires $\rho_c > 100\bar{\rho}_{\rm host}$. Together with Eq. (30) this implies that the minimum mass of a FDM solitonic system that survives 10 orbits at radius a inside a host of mass $\mathfrak{M}$ interior to a is given by

$$M > 6.7\times 10^8\ M_\odot\left(\frac{\mathfrak{M}}{10^{11}\ M_\odot}\right)^{1/4} \times\left(\frac{10\ {\rm kpc}}{a}\right)^{3/4}\left(\frac{10^{-22}\ {\rm eV}}{m}\right)^{3/2}. \tag{44}$$

This lower cutoff is consistent with numerical simulations [16], which find that halo substructure is suppressed below a few times $10^8\ M_\odot$.

The second reason why there are fewer FDM subhalos than CDM subhalos is that the power spectrum of FDM density perturbations is suppressed at small masses relative to CDM. We defer a discussion of this topic to Sec. IV.

The subhalo mass function can be probed in several ways. One approach is to look for gravitational lensing of background galaxies by the subhalos [104,105]. The strongest current limits come from ALMA observations

[11] A typical massive galaxy like the Milky Way has a circular speed of about 200 km s^{-1} so a satellite in a circular orbit of radius r completes $15(30\ {\rm kpc}/r)$ orbits in a Hubble time.

of high-redshift star-forming galaxies; at present these are only sensitive to subhalo masses $\gtrsim 10^9\ M_\odot$ [106], but technical advances should reduce this limit to the interesting range. A second is to study the evolution of tidal streams, which we discuss in the next subsection.

The too-big-to-fail problem arises when standard abundance matching methods to relate galaxies and halos are used to predict the magnitude difference between primary and secondary galaxies in groups. These studies [107,108] indicate that the expected number of luminous secondary galaxies is absent, and much work is being done to see if feedback from massive stars and black-hole outflows, or other baryonic physics, can account for the deficit. A fair, if brief, summary would be that while the latest high-resolution cosmological simulations [102] argue that the deficit will naturally be produced by radiatively driven winds and other feedback effects, considerably more work will need to be done by a variety of methods before this conclusion can be considered secure. In any event, FDM reduces the magnitude of the too-big-to-fail problem, both because the abundance of subhalos is smaller in FDM than CDM at all masses below $\sim 10^{10}\ M_\odot$ (Sec. IV) and because subhalo masses are generally estimated observationally by the maximum circular speed of the baryons, which is lower in FDM than CDM for halos of a given mass [109].

A more speculative concern is the origin of globular clusters (GCs), which remains mysterious. With typical stellar masses of $10^5\ M_\odot$ and sizes of roughly 10 pc, these old stellar systems surround all normal galaxies out to distances comparable to the virial radius. The total mass of GCs per galaxy seems to parallel the mass in dark matter more closely than the mass in baryons: the ratio of the mass in GCs to the mass in baryons is high at both ends of the galaxy mass spectrum, like the ratio of dark to baryonic mass. The presence of multiple stellar populations in GCs [110] also suggests that these systems had or have escape velocities large enough to retain gas. In an early paper before the existence of dark matter was widely recognized, Peebles and Dicke [111] speculated that GCs might have formed at the era of decoupling between matter and radiation, since they have the Jeans mass appropriate to that epoch ($z \simeq 10^3$). CDM has gravitationally unstable initial fluctuations on the scale of GCs but it is very difficult for the objects we see to have formed from these, for several reasons. First, the more massive subhalos (with halo mass of $10^8\ M_\odot$, say) are absent from our inventory of galaxies and their absence is explained in CDM by arguing that their relatively small escape velocities allow feedback to expel gas so efficiently that star formation is suppressed. If this explanation is correct, then the formation of stars in systems like GCs that are 100 times less massive would certainly be prohibited. Furthermore the expected sizes of the halos associated with GCs would be several kpc, so large that contraction of even very slowly rotating baryons to the present size of GCs would produce disk systems, whereas observed GCs are nearly spherical. Peebles has suggested [112] that in the CDM model GCs should be embedded in dark halos, but despite extensive searches [113–115] there have been no reports of diffuse dark matter in or around GCs. It is possible that the dynamics of FDM or other exotic alternatives to CDM could play a central role in the formation of these important but puzzling systems, but at the moment this is only a speculation.

H. Tidal streams

Subhalos affect the evolution of the tidal streams shed by globular clusters as they lose stars through external tidal forces and internal dynamical evolutionary processes [101]. The small-scale gravitational forces from subhalos can thicken, distort, and open gaps in streams; in extreme cases they may disperse the streams so rapidly that they disappear in much less than a Hubble time (see [116] for a review).

First consider stream thickening. Suppose for simplicity that all subhalos have the same mass m and size r_m, and that the number density of subhalos is N. If these move at speed v relative to the stream, the probability of an encounter with impact parameter smaller than b between a subhalo and a point on the stream in an interval t is

$$p = \pi N b^2 v t. \tag{45}$$

The differential tidal force across a stream of width w due to a mass m at distance r is $F = kGmw/r^3$ where k is of order unity, and integrating over the encounter yields an impulse $\Delta v = \int F dt = 2kGmw/(b^2 v)$. According to Eq. (45) the single closest encounter is given by $p = 1$ or $b_{\rm min}^2 = (\pi N v t)^{-1}$, and this gives an impulse[12]

$$\Delta v = 2\pi k w G N m t, \quad t \lesssim t_0. \tag{46}$$

An impulse Δv will cause the stream width to increase as $\dot{w} = \Delta v$. The derivation of (46) treats the subhalos as point masses, an approximation that is only valid when the minimum impact parameter is larger than the subhalo radius, $b_{\rm min} \gtrsim r_m$. Thus it is only valid up to a time $t_0 \equiv (\pi N v r_m^2)^{-1}$. At times smaller than this, the stream width will be dominated by the single closest encounter and if we assume this encounter occurs roughly midway through the time interval t then

$$w(t) \simeq w(0)\left(1 + \frac{1}{2}\pi k G N m t^2\right), \quad t \lesssim t_0. \tag{47}$$

Over times larger than t_0, stream thickening becomes a diffusive process due to encounters with many subhalos so

[12]Equation (46) is closely related to formulas for the disruption of binary stars due to tidal forces from massive objects such as molecular clouds [117,118].

Δv and w should be replaced by ensemble averages $\langle(\Delta v)^2\rangle^{1/2}$ and $\langle w^2\rangle^{1/2}$. A similar calculation yields

$$\frac{d\langle(\Delta v)^2\rangle}{dt} = \frac{4\pi(kGm)^2 N}{v r_m^2}\langle w^2\rangle, \quad t \gtrsim t_0. \tag{48}$$

Replacing $\langle(\Delta v)^2\rangle^{1/2}$ by $(d/dt)\langle w^2\rangle^{1/2}$ and integrating, we find

$$\langle w^2(t)\rangle^{1/2} = \langle w^2(t_0)\rangle^{1/2} \exp\left[\left(\frac{2\pi N k^2 G^2 m^2}{v r_m^2}\right)^{1/3}(t-t_0)\right], \quad t \gtrsim t_0. \tag{49}$$

Similar arguments can be used to derive the growth in the velocity dispersion of the stream.

Even a zero-thickness stream will be distorted by the gravitational impulse from passing subhalos. A zero-thickness stream is a one-dimensional manifold in phase space and must remain so; however it can be folded or crinkled so it appears to have nonzero thickness when projected onto a smaller number of phase-space dimensions (e.g., the two angular coordinates on the sky if it is detected as an overdensity in star counts). The statistical properties of this crinkling can be determined by recognizing that the gravitational force from a large number of subhalos can be approximated as a Gaussian random field that is homogeneous in time and space at small scales, although most investigations so far rely heavily, and appropriately, on simulations as well [119–122].

The dynamical effect of a subhalo on a stream that is easiest to detect is probably the opening of a "gap" by a close encounter with a single massive subhalo—strictly, this is a fold rather than a gap since as described above a zero-thickness stream is only distorted, not broken, by conservative forces [123,124].

Even once the effects of substructure are detected, it may be difficult to distinguish CDM from FDM, for several reasons: (i) most of the disruptive influence on streams comes from the most massive subhalos, which are present in both CDM and FDM [123]; (ii) substructure in the baryonic disk can also disrupt the streams [125]; (iii) in CDM the mass fraction in subhalos is a strong function of radius, typically ranging from a few percent at the virial radius, to 0.1% at 30 kpc, to 0.01% at $r < 10$ kpc [126]; (iv) numerical simulations suggest that many long, thin streams can survive for a Hubble time even in a CDM halo [127], so the difference between CDM and FDM will lie in the abundance of old streams rather than their presence or absence.

Despite these concerns, we note that the power of tidal streams to discriminate among halo models will improve dramatically over the next several years with astrometry from the Gaia spacecraft, which will discover many more streams and provide much more accurate kinematic observations of them.

I. Galactic disks

The relaxation time (32) is sufficiently short that solitonic "dark disks" could coalesce around the inner parts of baryonic galactic disks.

A useful first approximation to the structure of solitonic disks is obtained by neglecting the baryonic contribution to the gravitational potential and computing the ground state of the Schrödinger-Poisson equation in one dimension [Eq. (B1) with $\nabla^2 \to d^2/dz^2$]. The density $\rho_{\rm FDM}(z)$ in this state is symmetric around $z = 0$ and can be characterized by the central density $\rho_{\rm FDM}(0)$; the surface density $\Sigma_{\rm FDM} = \int_{-\infty}^{\infty} dz \rho_{\rm FDM}(z)$; and the half-thickness $z_{1/2}$, defined by $\int_0^{z_{1/2}} dz \rho_{\rm FDM}(z) = \frac{1}{2}\int_0^{\infty} dz \rho_{\rm FDM}(z)$. We find

$$\begin{aligned}\rho_{\rm FDM}(0) &= 0.984\left(\frac{G\Sigma_{\rm FDM}^4 m^2}{\hbar^2}\right)^{1/3} \\ &= 0.104\ M_\odot\,{\rm pc}^{-3}\left(\frac{\Sigma_{\rm FDM}}{100\ M_\odot\,{\rm pc}^{-2}}\right)^{4/3} \\ &\quad\times\left(\frac{m}{10^{-22}\ {\rm eV}}\right)^{2/3} \\ z_{1/2} &= 0.2744\left(\frac{\hbar^2}{G\Sigma_{\rm FDM} m^2}\right)^{1/3} \\ &= 260\ {\rm pc}\left(\frac{100\ M_\odot\,{\rm pc}^{-2}}{\Sigma_{\rm FDM}}\right)^{1/3}\left(\frac{10^{-22}\ {\rm eV}}{m}\right)^{2/3}.\end{aligned} \tag{50}$$

In the solar neighborhood, the total surface density within ± 1.1 kpc of the Galactic midplane is $68 \pm 4\ M_\odot\,{\rm pc}^{-2}$, of which $51 \pm 4\ M_\odot\,{\rm pc}^{-2}$ is composed of baryons (gas and stars) [128]. The total density in the Galactic midplane is $\rho(0) = 0.10 \pm 0.01\ M_\odot\,{\rm pc}^{-3}$, most or all of which is baryonic [129]. The first of these results implies that at most $20\ M_\odot\,{\rm pc}^{-2}$ is present in a dark-matter disk; then Eq. (50) implies that for $m = 10^{-22}$ eV, $z_{1/2} \gtrsim 450$ pc and $\rho(0) \lesssim 0.012\ M_\odot\,{\rm pc}^3$, large enough and small enough respectively that the assumption that the solitonic disk dominates the gravitational potential is inconsistent.[13]

In the opposite limit, the gravitational potential is dominated by baryons rather than FDM. Since the scale height of the solitonic disk is large, we can approximate the baryonic contribution as arising from a zero-thickness sheet of surface density Σ_b. Then

[13] An unrelated problem with a solitonic disk of this kind is that it is likely unstable at horizontal wavelengths that are large compared to its thickness.

$$\rho_{\rm FDM}(0) = 1.141\frac{\Sigma_{\rm FDM}}{\Sigma_b}\left(\frac{G\Sigma_b^4 m^2}{\hbar^2}\right)^{1/3} = 0.120\ M_\odot\,{\rm pc}^{-3}\frac{\Sigma_{\rm FDM}}{\Sigma_b}\left(\frac{\Sigma_b}{100\ M_\odot\,{\rm pc}^{-2}}\right)^{4/3} \times\left(\frac{m}{10^{-22}\ {\rm eV}}\right)^{2/3}$$
$$z_{1/2} = 0.2399\left(\frac{\hbar^2}{G\Sigma_b m^2}\right)^{1/3} = 228\ {\rm pc}\left(\frac{100\ M_\odot\,{\rm pc}^{-2}}{\Sigma_b}\right)^{1/3}\left(\frac{10^{-22}\ {\rm eV}}{m}\right)^{2/3}. \quad (51)$$

Taking $\Sigma_b = 51\ M_\odot\,{\rm pc}^{-2}$ and $\Sigma_{\rm FDM} = 17\ M_\odot\,{\rm pc}^{-2}$ we obtain $\rho_{\rm FDM}(0) = 0.016\ M_\odot\,{\rm pc}^{-3}(m/10^{-22}\ {\rm eV})^{2/3}$ and $z_{1/2} = 285\ {\rm pc}(m/10^{-22}\ {\rm eV})^{-2/3}$. We conclude that a possible solitonic disk of FDM with $m = 10^{-22}$ eV has thickness comparable to the baryonic disk and makes only a small ($\lesssim$20%) relative contribution to the density in the solar neighborhood; for $m = 10^{-21}$ eV the central density would be comparable to the density of stars and gas and the disk would be thinner than the stellar disk. For comparison, the local density expected from a CDM halo is $\sim$0.01 $M_\odot\,{\rm pc}^{-3}$ [130]. The thin dark disk proposed by [131], with surface density $\sim$10 $M_\odot\,{\rm pc}^{-2}$ and thickness $\sim$10 pc, could not be composed of FDM unless the particle mass $m \gtrsim 5\times10^{-20}$ eV, much too large to explain the other small-scale structure issues addressed in this paper.

J. Dynamical friction

The only low-luminosity satellite galaxy of the Milky Way that contains globular clusters is the Fornax dwarf spheroidal, the most luminous satellite in this class, which has five. The time scale for orbital decay of a point mass m in a background of density ρ and velocity dispersion σ is roughly $\sigma^3/(G^2\rho m)$ [55,132]. The mass density in Fornax is high enough, and the velocity dispersion low enough, that dynamical friction should have caused most of the clusters to spiral to the center of the galaxy and merge to form a prominent nucleus, which is not seen [133]. A similar problem is present in faint dwarf elliptical galaxies in several nearby galaxy clusters [134]. Various explanations have been put forward to explain the discrepancy (e.g., [135]); the most widely discussed possibility is that the drag from dynamical friction is reduced, eliminated, or even reversed if the stellar system hosting the clusters has a homogeneous (constant-density) core. This effect, sometimes called "core stalling," is seen in a variety of N-body simulations [75,136,137] but the physics behind it remains murky [136,138,139].

Here we ask how dynamical friction is modified if the dark matter in dwarf galaxies is comprised of FDM rather than CDM [13]. There are three distinct effects: (i) many exotic dark-matter models, including FDM, produce cores at the centers of halos rather than the central cusp found in CDM [8,140–145] and thus modify the rate of orbital decay according to the classic Chandrasekhar formula [132] through changes in the dark-matter density and velocity dispersion, the orbital speed, etc.; (ii) as reviewed above, core stalling can reduce or eliminate the drag from dynamical friction in a homogeneous core compared to the value predicted by Chandrasekhar; (iii) standard estimates of the drag from dynamical friction must be modified to account for the large de Broglie wavelengths of FDM particles, as shown in Appendix D. Here we focus on the last of these effects, also investigated by [146].

The orbital decay time scale for an object of mass $m_{\rm cl}$ in a circular orbit of radius r in a host system of density $\rho(r)$ and enclosed mass $\mathfrak{M}(r)$ is given by Eq. (D16),

$$\tau = \frac{37.5\ {\rm Gyr}}{C}\left(\frac{\mathfrak{M}(r)}{10^8\ M_\odot}\frac{1\ {\rm kpc}}{r}\right)^{3/2}\frac{10^5\ M_\odot}{m_{\rm cl}}\frac{0.01\ M_\odot\,{\rm pc}^{-3}}{\rho(r)}, \quad (52)$$

where the dimensionless constant C is plotted in Fig. 2, and the fiducial values have been chosen to approximately match Fornax and its globular clusters. For a more careful comparison between frictional decay times in FDM and CDM we adopt masses for the five Fornax clusters from [137] and set their orbital radii equal to the projected radii from the center of Fornax multiplied by $2/\sqrt{3}$ (the ratio of the radius to the median projected radius in a spherical distribution). For CDM (i) we take the Fornax density from the "steep cusp" model of [137], which has a logarithmic density slope near the center $d\log\rho/d\log r = -1$ as in the NFW profile [3] that characterizes CDM halos. (ii) We set the constant C in Eq. (52) to $0.5\log[2v^2r/(Gm_{\rm cl})]$ following Eq. (D11); the factor 0.5 is a crude empirical correction that arises because the classical dark-matter particles have velocities comparable to the globular clusters and only particles traveling slower than the test object contribute to the frictional force [55]. For FDM we use the "large core" model of [137], and determine C from Eq. (D14) using $k = mv/\hbar$ where the velocity v is determined by assuming the cluster is on a circular orbit.

The resulting decay times are shown in Table I for a particle mass of 3×10^{-22} eV. In all cases shown in the table the orbital decay times are longer in a FDM halo than in a CDM halo. The shortest decay time in the FDM halo exceeds 2 Gyr, compared to 0.4 Gyr in the CDM halo. Four of the five clusters have decay times of 10 Gyr or more in the FDM halo, thus solving the puzzle of why the

TABLE I. Orbital decay times for the globular clusters in Fornax for CDM and FDM. Notes: Projected separations and globular cluster masses are taken from [137]. Orbital decay times τ are determined from Eq. (D16) using the steep cusp and large core density distributions from [137] for CDM and FDM respectively. The dimensionless wave number $kr = mvr/\hbar$ is evaluated assuming $m = 3 \times 10^{-22}$ eV and $v^2 = G\mathfrak{M}(r)/r$, appropriate for a circular orbit. The dimensionless constant C is determined using Eq. (D14) for FDM, and as described in the text for CDM.

	Projected radius	Cluster mass	CDM		FDM		
n	$r_\perp$ (kpc)	$m_{\rm cl}$ ($M_\odot$)	C	τ (Gyr)	kr	C	τ (Gyr)
1	1.6	3.7×10^4	4.29	112	8.90	2.46	215
2	1.05	1.82×10^5	3.32	9.7	5.04	1.88	12
3	0.43	3.63×10^5	2.45	0.62	0.97	0.29	2.2
4	0.24	1.32×10^5	2.50	0.37	0.31	0.033	10
5	1.43	1.78×10^5	3.46	21.3	7.79	2.32	31

globular clusters in Fornax have survived. For other particle masses the decay time scales roughly as m^{-2} for clusters 3 and 4, which have the smallest orbits and the shortest decay times. Observations of a larger sample of dwarf galaxies containing globular clusters could further test the possibility that dynamical friction is suppressed compared to the expectations from CDM. Note that the dynamical friction issue could in principle be decoupled from the issue of predicting the density profile. With sufficiently high quality data, the density profile of the host galaxy can be observationally determined, sidestepping debates about the impact of baryonic effects. Given the measured profile, CDM or FDM makes predictions for the dynamical friction time scale that can be checked against observations.

Dynamical friction from a CDM halo is also expected to drain the angular momentum from the central bar found in the majority of disk galaxies [147–153]. This expectation is in tension with the observation that most bars are rapidly rotating, in that the corotation radius is not far outside the outer edge of the bar [154]. This tension could be resolved if the dark matter is efficiently trapped into resonances with the bar [155], or if the halo has a large core radius so the density of the halo within several kpc of the galaxy center is lower than expected from CDM. The FDM hypothesis could contribute to the resolution of this problem since friction would also be reduced if the half-mass radius of the central FDM core were larger than the bar radius ($kr \lesssim 1$ in Fig. 2).

K. The most massive halos

The virial masses of the large halos associated with the richest clusters of galaxies approach $M_{\rm vir} = 1$–$2 \times 10^{15}\ M_\odot$, If the relation (31) can be extrapolated to these large halo masses, it implies a central soliton mass

$$M \simeq 1.3 \times 10^{10}\ M_\odot \frac{10^{-22}\ \text{eV}}{m} \left(\frac{M_{\rm vir}}{10^{15}\ M_\odot}\right)^{1/3}. \quad (53)$$

This is still well below the maximum soliton mass for FDM particles with no self-interactions [Eq. (43)]. The corresponding half-mass radius is given by Eq. (29),

$$r_{1/2} \simeq 25\ \text{pc} \frac{10^{-22}\ \text{eV}}{m} \left(\frac{10^{15}\ M_\odot}{M_{\rm vir}}\right)^{1/3}. \quad (54)$$

Structures with this mass and size would be a unique signature of FDM. We have argued in Sec. III C that the extrapolation yielding Eq. (53) probably overestimates the soliton mass at large halo masses, but it is worthwhile to investigate the observable consequences that would result if this extrapolation were correct.

We first ask whether dense solitons at cluster centers might already have been detected, but interpreted as supermassive black holes. The nearest moderately rich cluster is the Virgo cluster. The luminous galaxy M87 is located near the center of the cluster and contains a central dark object of mass $(6.6 \pm 0.4) \times 10^9\ M_\odot$ as determined by observations of stellar kinematics [156]. The resolution of these observations is about 0.2–0.3 arcsec or 17–25 pc and the upper limit to the size of the central object is probably twice as large. For comparison, the soliton in a halo of mass $M_{\rm vir} \simeq 2 \times 10^{14}\ M_\odot$, roughly appropriate for Virgo, would have $M \simeq 7 \times 10^9 (10^{-22}\,\text{eV}/m) M_\odot$ and $r_{1/2} \simeq 40 (10^{-22}\ \text{eV}/m)$ pc, roughly consistent with these observations. A second prominent cluster is the Coma cluster, about five times more distant than Virgo. The luminous galaxy NGC 4889 near the center of Coma has a central dark object of mass 0.6–$3.7 \times 10^{10}\ M_\odot$ [157]. The spatial resolution of these observations is ~100 pc so the soliton expected to form at the center of Coma could easily masquerade as a black hole. Despite these appealing numerical coincidences, we do not favor the hypothesis that the central dark objects in M87 and NGC 4889 are solitons rather than black holes. There is an active galactic nucleus and a relativistic jet at the center of M87 and a wide range of observational evidence and theoretical arguments suggests that these phenomena are always associated with black holes. Moreover, the masses are similar to those of central dark objects in other galaxies with similar properties that are at the centers of rich clusters [158].

Where, then, are the massive, dense solitons predicted by FDM? There are two main possibilities: (i) The galaxies we have examined may not be at the centers of their respective cluster halos. The Virgo cluster has a double structure, and although M87 is in the core of the denser subcluster it is displaced from its center in both position and velocity [159]. The Coma cluster also appears to consist of two

subclusters that have not yet relaxed into equilibrium [160]. (ii) As we have discussed, the soliton mass–virial mass relation in Eqs. (31) and (53) may overestimate the soliton mass at the halo masses $\sim 10^{15}\ M_\odot$ considered here. For example, Eq. (32) implies that in a halo with typical velocity $v = 10^3\ \mathrm{km\,s^{-1}}$, typical for rich clusters, the relaxation time is less than 10^{10} yr only at radii $r \lesssim 1.5\ \mathrm{kpc}\ f_{\mathrm{relax}}^{1/4}(10^{-22}\ \mathrm{eV}/m)^{3/4}$, and the halo mass inside that radius is insufficient to produce a soliton of $10^{10}\ M_\odot$.

A related question is whether the soliton can survive if there is a supermassive black hole at its center. A nonrotating black hole of mass $M_\bullet$ traveling at speed v through a uniform scalar field of mass m and density ρ accretes mass at a rate [161]

$$\frac{dM_\bullet}{dt} = \frac{32\pi^2 (GM_\bullet)^3 m\rho}{\hbar c^3 v[1-\exp(-\xi)]}, \quad \text{where } \xi = \frac{2\pi G M_\bullet m}{\hbar v} \tag{55}$$

$$= \begin{cases} \frac{16\pi (GM_\bullet)^2 \rho}{c^3}, & \xi \ll 1, \\ \frac{32\pi^2 (GM_\bullet)^3 m\rho}{\hbar c^3 v}, & \xi \gg 1. \end{cases} \tag{56}$$

For an approximate analysis we take ρ and v to be the central density and virial velocity of the soliton [Eqs. (B3) and (B4)]. Then

$$\xi = 19.07 \frac{M_\bullet}{M} \tag{57}$$

where M is the soliton mass, independent of the mass of the FDM particle. The mass accretion rate is

$$\frac{dM_\bullet}{dt} = \begin{cases} \frac{2.5\times 10^7\ M_\odot}{10^{10}\ \mathrm{yr}} \left(\frac{M_\bullet}{10^9\ M_\odot}\right)^2 \left(\frac{m}{10^{-22}\ \mathrm{eV}}\right)^6 \left(\frac{M}{10^{10}\ M_\odot}\right)^4, & \xi \ll 1 \\ \frac{4.75\times 10^7\ M_\odot}{10^{10}\ \mathrm{yr}} \left(\frac{M_\bullet}{10^9\ M_\odot}\right)^3 \left(\frac{m}{10^{-22}\ \mathrm{eV}}\right)^6 \left(\frac{M}{10^{10}\ M_\odot}\right)^3, & \xi \gg 1. \end{cases} \tag{58}$$

From the first of these equations we find that a seed black hole of mass $M_{\bullet i} \ll M$ grows to $\xi \sim 1$ in a time

$$t = 4\times 10^{14}\ \mathrm{yr} \left(\frac{10^{-22}\ \mathrm{eV}}{m}\right)^6 \frac{10^6\ M_\odot}{M_{\bullet i}} \left(\frac{10^{10}\ M_\odot}{M}\right)^4. \tag{59}$$

For the nominal parameters this rate is negligible; i.e., small seed black holes embedded in the soliton do not grow significantly. However, the rate depends strongly on the particle mass and could be significant for $m \gtrsim 5\times 10^{-22}$ eV. Once the soliton contains a black hole more massive than a few percent of the soliton mass, so $\xi \gg 1$, the last of Eqs. (58) implies that a black hole of initial mass $M_{\bullet i}$ swallows the soliton on a time scale

$$t = 1\times 10^{11}\ \mathrm{yr} \left(\frac{10^{-22}\ \mathrm{eV}}{m}\right)^6 \left(\frac{10^9\ M_\odot}{M_{\bullet i}}\right)^2 \left(\frac{10^{10}\ M_\odot}{M}\right)^3. \tag{60}$$

Once again, this rate is not important for the nominal parameters but could be significant for particle masses a few times larger than the nominal value of 10^{-22} eV.

IV. FDM AND GALAXY FORMATION

In contrast to CDM, in which small density fluctuations are unstable on all spatial scales inside the horizon, FDM is unstable only for masses larger than the Jeans mass, Eq. (42). As discussed in Sec. III E, the Jeans mass defines a lower limit to the mass of FDM halos and subhalos.

A stronger, but cosmology-dependent, constraint on the abundance of halos in FDM arises because the linear power spectrum of density fluctuations in FDM is suppressed relative to CDM at small scales. The degree of suppression is expressed by the ratio of the FDM power spectrum to the CDM power spectrum. This ratio at $z = 0$ is less than 0.5 for wave numbers greater than and halo masses less than [12,162]

$$k_{1/2} = 4.5\ \mathrm{Mpc}^{-1} \left(\frac{m}{10^{-22}\ \mathrm{eV}}\right)^{4/9}, \tag{61}$$

$$M_{1/2} = \frac{4}{3}\pi\rho \left(\frac{\pi}{k_{1/2}}\right)^3 = 5\times 10^{10}\ M_\odot \frac{\Omega_{\mathrm{FDM}}}{0.27} \left(\frac{10^{-22}\ \mathrm{eV}}{m}\right)^{4/3}. \tag{62}$$

Linear theory therefore predicts a sharp cutoff in the initial masses of FDM structures considerably above the limit given by Eqs. (39) or (42). However, nonlinear numerical computations show that these overdensities fragment, leaving a spectrum of lower-mass self-gravitating objects down to the scale given by those two equations, in which the number density of subhalos is reduced in FDM relative to CDM by a factor $\sim (3M/M_{1/2})^{2.4}$ [162]. It is important to verify these conclusions with different simulations and different numerical techniques, but for now we assume that they are correct.

These arguments show that FDM tends to suppress formation of small galaxies at high redshift compared to CDM. Thus it becomes a serious question as to whether the FDM model would allow galaxies to be formed that were capable of reproducing the high-redshift galaxy luminosity function, reionizing the Universe at $z = 8$–9 [163], and producing the early, small-scale structure probed by the Lyman-α forest.

Because the power spectrum of density fluctuations in FDM is suppressed for halo masses much larger than the Jeans mass ($M_{1/2} \gg M_J$) one can approximate the

formation of structure in FDM using CDM simulations in which the initial power spectrum is that of FDM (although of course this approximation cannot capture the formation of solitons at the centers of these halos). Using this approach, Schive *et al.* [162] and [164] have shown that FDM can reproduce the UV luminosity function of galaxies in the redshift range 4–10, assuming a plausible relation between galaxy luminosity and halo mass, if $m > 10^{-22}$ eV. They also show that FDM is consistent with current observations of the reionization history for plausible estimates of the production rate of ionizing photons, about three times larger than required for CDM.[14]

V. LYMAN-ALPHA FOREST CONSTRAINTS ON WDM AND FDM

The Lyman-α forest offers an additional probe of the power spectrum. Viel *et al.* [19] examined constraints on warm dark matter from the forest and concluded that the mass of a hypothetical WDM particle must exceed $m_{\rm FDM} = 3.3$ keV at the 2-σ level. The 3-σ, 4-σ and 9-σ lower limits are 2.5,2 and 1 keV respectively. WDM and FDM do not have exactly the same matter power spectrum. However, they share the same power spectrum at large scales, and both exhibit a precipitous drop in power below a respective characteristic scale. Thus we can roughly translate an observational bound on WDM to a corresponding one on FDM by matching $k_{1/2}$ for FDM from Eq. (61)[15] to the analogous quantity for WDM [19,109],[16]

$$k_{1/2} = 12.5\ {\rm Mpc}^{-1}\left(\frac{m_{\rm FDM}}{2.5\ {\rm keV}}\right)^{1.11}\left(\frac{\Omega_{\rm FDM}}{0.27}\right)^{-0.11} \times \left(\frac{H_0}{70\ {\rm km\,s^{-1}\,Mpc^{-1}}}\right)^{2.22}. \quad (63)$$

A WDM mass of 1,2,2.5,3.3 keV translates into a FDM mass $m \sim 1, 6, 10, 20 \times 10^{-22}$ eV respectively. Thus the range of FDM masses we are interested in is disfavored by the Lyman-α forest data, and strongly so at the low-mass end. It would be useful, however, to verify this conclusion with actual FDM numerical simulations of the forest. It is possible that FDM has density fluctuations on scales relevant to the forest (see Sec. III C and [16]) that are not present in a WDM model. It is also prudent to examine the assumptions underlying the WDM constraints, which we now do.

It has been understood starting from the 1990s that the statistical properties of the Lyman-α forest can be explained by the ΛCDM model with a minimal set of additional assumptions [166–173]. The most important of these is that the neutral hydrogen density $n_{\rm HI}$ responsible for the Lyman-α absorption obeys

$$n_{\rm HI} \propto (1+\delta_b)^2 T^{-0.7} J^{-1} \quad (64)$$

where δ_b is the fractional overdensity of baryons; T is the temperature; and J is the amplitude of the ionizing background (suitably averaged over frequencies, weighted by the ionization cross section). Photoionization equilibrium is assumed to be a good approximation, which leads to the factors of $(1+\delta_b)^2$ (the ionized fraction is close to unity) and $T^{-0.7}$ (approximate scaling of the recombination rate with the temperature). There is a tight correlation between temperature and density in a low-density photoionized medium, $T = T_0(1+\delta_b)^{\gamma-1}$, where $\gamma \sim 1$–1.6 [174]. It is generally assumed that T_0, γ and J have negligible spatial fluctuations; fluctuations in $n_{\rm HI}$ thus reflect fluctuations in baryon density δ_b. The baryon fluctuations in the intergalactic medium are assumed to evolve under gravity, counteracted by pressure. Feedback processes, such as galactic winds or outflows, are assumed to have negligible impact on the forest.

Lyman-α constraints on WDM fall into two categories: those that are primarily from high-redshift, high-resolution data, and those that come from data at lower redshifts and larger scales. We start with a discussion of the first category, exemplified by the thorough analysis of Viel *et al.* [19], who derived constraints from data at $z \sim 4.2$–5.4 covering scales $k \sim 0.4$–$9\ {\rm Mpc}^{-1}$. Their strongest constraint comes from the highest redshifts, $z \sim 5.4$, and the smallest scales, $k \sim 4$–$9\ {\rm Mpc}^{-1}$ (see Fig. 12 of [19]). WDM with a mass of 2.5 keV causes a 10% suppression of power on these scales, in tension with the data.[17] At high redshifts, two effects are potentially significant: (i) the larger average neutral hydrogen density and the smaller number of ionizing sources leads to enhanced spatial fluctuations of the ionizing background J, and (ii) there can be significant fluctuations in the temperature, remnants of an inhomogeneous reionizing process as one approaches the epoch of reionization (recent Planck constraints suggest reionization on average occurred around $z \sim 8$ [163]).

[14]These results are consistent with a semianalytic study by Bozek *et al.* [165], once these calculations are updated to use the 2016 Planck value for the reionization optical depth [163].

[15]We thank Rennan Barkana for a private communication on this point, and for discussions on the impact of reionization on WDM/FDM constraints. The procedure of matching $k_{1/2}$ was also discussed in [109].

[16]We focus on $m_{\rm WDM} = 2.5$ keV as this case is treated in detail by Viel *et al.*.

[17]Keeping all other parameters fixed, at this mass, scale and redshift WDM suppresses the power by ∼50%. However, by allowing other parameters (such as the temperature) to vary to best fit the data, the net suppression is closer to ∼10%. Note that $k_{1/2}$ in Eq. (63) refers to the suppression scale for the linear matter power spectrum; the nonlinear mapping from mass to flux moves the suppression scale to a lower k for the flux power spectrum.

An attempt was made by Viel *et al.* to account for the first effect using a simulation in which the ionizing background is sourced by rare quasars, with the accompanying clustering and Poisson fluctuations. However, the simulation did not include spatial fluctuations due to the inhomogeneous distribution of absorbers. There appears to be a variety of possible modifications to the flux power spectrum from a fluctuating ionizing background, depending on assumptions about the density and clustering of the ionizing sources and absorbers. For instance, the authors of [175] showed that while quasars as sources tend to add power at large scales without significantly affecting the small-scale power, Lyman-break galaxies tend to suppress power at large scales $k \sim 0.1$–$0.5\ \mathrm{Mpc}^{-1}$ and add power at small scales $k \gtrsim 1\ \mathrm{Mpc}^{-1}$, especially at high redshifts (see Figs. 5 and 7 of [175]). Even in the case of quasars as sources, different investigators arrive at different conclusions about the scale dependence of the flux power spectrum modification (for instance the author of [176] included inhomogeneous radiative transfer, and the authors of [175,177] applied an average attenuation). In fitting the forest data, the common practice is to assume a template for the effect of a fluctuating ionizing background—meaning the *shape* (scale dependence) of the flux power spectrum modification—and allow the *amplitude* of the modification to be a free parameter. In this way, the authors of [19] obtained a bound on the amplitude of a particular quasar template, and showed that it does not have a large impact on the WDM constraint. It would be useful to repeat the analysis using other templates, including those that might be more degenerate with the effect of WDM in their scale dependence (such as those from galaxies as ionizing sources, and those that account for inhomogeneous radiative transfer).

The second astrophysical effect to consider is spatial fluctuations in temperature due to patchy reionization. Reionization typically raises the temperature of the intergalactic medium to a few times 10^4 K. The gas generally cools afterwards (except for late time HeII reionization that could temporarily reverse this trend). Because different patches of the medium reionize at different times due to fluctuations in the distribution of ionizing sources and absorbing materials, the temperature could vary by a factor of a few at redshift ~ 5 if the reionization of different patches spans the redshift range ~ 7–10 [178,179]. Let us stress that by temperature variations, we are not referring to the fact that temperature depends on density—such a dependence is expected, even in the absence of inhomogeneous reionization, and is captured by the temperature-density relation $T = T_0(1+\delta_b)^{\gamma-1}$ described earlier. Here we are interested in an extra source of fluctuations in temperature. It can be described in a number of ways. One way is to phrase this in terms of fluctuations in temperature that exist even at the same local density, say the mean density T_0.[18] A more sophisticated description would correlate the local temperature to the density smoothed on a larger scale (the scale of the reionization patch). A patch with a higher large-scale density might reionize earlier, due to an abundance of sources, leading to a lower temperature at the observed redshift. The opposite could happen: the same patch might reionize later, due to shielding by an abundance of absorbers, leading to a higher temperature.

Less attention has been paid to this second effect, that of patchy reionization on the flux power spectrum. An exception is [180],[19] whose authors compared how two simulations, with early and late reionization respectively, predict different flux power spectra at $z \gtrsim 4$. They found that the late reionization scenario increases the power at large scales $k \lesssim 5\ \mathrm{Mpc}^{-1}$ and suppresses it at small scales $k \gtrsim 5\ \mathrm{Mpc}^{-1}$. Could further investigations, exploring different assumptions about the sources and absorbers, reveal qualitatively different behavior, just as in the case of the first effect? Let us describe one possibility, motivated by the observations of D'Aloisio *et al.* [179].

By examining the average absorption at $z \sim 5.5$–5.9 along different lines of sight, D'Aloisio *et al.* found evidence that T_0 fluctuates on a scale of ~ 36 Mpc, suggesting reionization patches of this size. Such fluctuations leave two imprints on the flux power spectrum. Fluctuations in temperature lead to fluctuations in the recombination rate, and therefore in the neutral hydrogen density [Eq. (64)]. The affected scale is roughly $k \lesssim \pi/36\ \mathrm{Mpc} \sim 0.09\ \mathrm{Mpc}^{-1}$; this is beyond the largest scales probed in existing 1D power spectrum analyses [181]. Cross power spectra might be useful in this respect. A second imprint, perhaps surprisingly, is present at small scales, and arises because of smoothing. There are two known sources of smoothing, thermal broadening (an effect in 1D) and gas pressure, i.e., Jeans smoothing (an effect in 3D). Thermal broadening dominates the smoothing of the observed (1D) flux power spectrum [182,183], although for our purpose there is no real need to distinguish between the two. A finite temperature leads to a smoothing of the flux power spectrum: $P_f(k) \to P_f(k)W(k,T_0)$, where $W(k,T_0)$ is the smoothing kernel.[20] At a temperature around 10^4 K, the smoothing kernel suppresses power at $k \gtrsim 5\ \mathrm{Mpc}^{-1}$;

[18] At redshift $\gtrsim 5$, the relevant density is actually $\delta_b < 0$ for pixels that are not completely saturated. We use the temperature at the mean density T_0 as a convenient proxy, since spatial fluctuations in T_0 imply temperature fluctuations at another density too. It is worth emphasizing that inhomogeneous reionization leads to spatial fluctuations in the exponent γ and in fact the whole temperature-density relation.

[19] We thank Uros Seljak for pointing out this and other references, and for thoughtful discussions on the Lyman-α forest.

[20] The smoothing kernel strictly speaking should depend on γ and even reionization history [171], in addition to T_0. We use T_0 as a proxy for the dependence of the smoothing kernel on the thermal state of the gas.

the higher the temperature, the larger the affected scales. A measurement of the flux power spectrum from many reionization patches effectively probes the *averaged* smoothing kernel $\langle W(k, T_0)\rangle$. This need not be the same as the smoothing kernel at the averaged temperature $W(k, \langle T_0\rangle)$. In general $\langle W(k, T_0)\rangle$ might even differ in shape from the smoothing kernel at *any* temperature. We expect $\langle W(k, T_0)\rangle$ to retain more small-scale power: at high k's, the power is dominated by patches where the temperature fluctuates below the mean. The magnitude of this effect depends on the range of temperature in these reionization patches. We estimate that the effect could be at the $\sim$10% level on scales relevant for the WDM constraint, if the difference between the highest and lowest temperatures exceeds 10^4 K. It would be useful to investigate this more carefully using numerical simulations.

It is worth noting that, the effect of patchy reionization aside, simply modifying the thermal history could impact the WDM constraint also. It was shown by [184] that allowing for a nonmonotonic temperature evolution (expected if HeII reionization occurs at intermediate redshifts) weakens the 2σ lower bound on the WDM mass from 3.3 keV to 2.1 keV, using the same data as [19].

We close by discussing WDM constraints from Lyman-α forest data at large scales and low redshifts ($k \sim 0.06$–1.6 Mpc^{-1}, $z \sim 2.2$–4.4), for instance Seljak *et al.* [185], and more recently, Baur *et al.* [186]—the latter gave a 2σ lower limit of $m_{\rm WDM} > 4.1$ keV. At these lower redshifts, the effects discussed above, patchy reionization and fluctuations in the ionizing background, are reduced. On the other hand, the effect of WDM is also smaller on these relatively large scales: the difference in power between CDM and WDM ($m_{\rm WDM} = 2.5$ keV for instance) is at the few percent level if the other parameters are fixed [186]; allowing them to float to their respective best-fit values would further diminish the difference between the two models. At this level of precision, the effect of fluctuations in the ionizing background might not be negligible. Moreover, [187] showed that galactic outflows can also impact the flux power spectrum at this level (see also [188]). Typically, these astrophysical effects are accounted for by template fitting: a template based on numerical simulations of the effect is introduced which fixes the scale (and often redshift) dependence of the flux power modification; the amplitude of the modification is treated as a free parameter, and WDM constraints are obtained by marginalizing over this parameter. As emphasized earlier in the context of fluctuations in the ionizing background, it is helpful to explore the diversity of possible templates. In the case of galactic outflows, it would be useful to know how robust the assumed redshift and scale dependence is to uncertainties in the physics of galaxy formation.

In summary, it is possible that the existing Lyman-α forest constraints on WDM would be relaxed if the diversity of modifications to the flux power spectrum, from a number of astrophysical effects, is taken into account. We believe effects similar to those we have discussed could weaken the corresponding FDM lower bound to a few times 10^{-22} eV. Further analyses of simulations and data are required to determine if this is the case. It would also be helpful to carry out the flux power spectrum analyses directly on FDM simulations, to test the validity of (or to bypass) the translation between WDM and FDM constraints.

VI. SUMMARY

The standard lambda cold dark matter or ΛCDM model for the nature of dark matter and the growth of cosmic structure in the Universe describes a wide variety of observations with remarkable precision. To date, experimental searches for the particle or particles comprising CDM have been unsuccessful or controversial, but "absence of evidence is not evidence of absence" and many ongoing experiments offer the hope of future success. A larger concern is that few if any of the predictions of the CDM scenario on scales smaller than $\sim$10 kpc have been successful. While all large-scale predictions of ΛCDM appear to be valid, the simple-minded predictions of this model are inconsistent with the relatively small number of low-mass field and satellite galaxies, the absence of dark-matter cusps at the centers of galaxies dominated by dark matter, the absence of dark matter around normal globular clusters, the weakness of dynamical friction in dwarf galaxies, and several other phenomena. Complex dynamics or baryonic physics may ultimately prove able to account for all of these, but it is worthwhile to investigate whether some well-motivated model for the properties of the dark matter could replicate the successes of CDM at large scales and in addition predict properties of the dark-matter distribution and dynamics at small scales (and correspondingly at early times) that are in better agreement with the observations than is CDM.

One possibility that has been considered by a number of investigators is an extremely light boson having a de Broglie wavelength λ of kpc scale at the typical internal velocities in galaxies [Eq. (18)]. A fluid with these properties would resist compression to smaller scales and could not form equilibrium self-gravitating halos with mass smaller than about $10^7\ M_\odot$ [Eqs. (39) and (42)], so it provides a model that is eminently falsifiable by comparison to observations at early times and small scales. We have summarized the work of others (see also the recent review by Marsh [17]) and added several new calculations, concluding that, if the particle mass lies in the range $m = 1$–10×10^{-22} eV, the FDM scenario is an attractive alternative to CDM with new and powerful tests soon to be available and new calculations and simulations needed to elucidate its behavior. For several of the astrophysical applications the lower end of this mass range is preferable

but current observations of the Lyman-α forest, though their interpretation is somewhat model dependent, favor the upper end of the range and may require masses as large as $10\text{–}20 \times 10^{-22}$ eV. We note in the text and in what follows the many possible observations that could cleanly demonstrate that FDM is not the dominant form of dark matter.

A possible concern is that it is unnatural to have a boson with a mass $\sim 10^{-22}$–10^{-21} eV, many orders of magnitude less than the masses of known elementary particles. In fact, a spinless field of very small mass that also interacts very weakly with ordinary matter is fairly natural in particle physics, because there is extra symmetry in the limit of a massless field of spin zero that interacts only with gravity. Moreover, there are natural mechanisms to generate a nonzero but exponentially small mass for such a field. In models with multiple fields of this type, which are relatively well motivated (see for example [23]), it is plausible that one of these fields might have a mass in the required range [see Eq. (13)].

Simulations show that FDM halos are comprised of an envelope that resembles the NFW profile found in CDM [3], surrounding a central core or peak that is a stationary, minimum-energy solution of the Schrödinger-Poisson equation, sometimes called a "soliton." As described in Sec. III C, the density of the soliton can be much larger than the density of the surrounding halo, and produces a distinct signature in the rotation curve of FDM-dominated systems that contain baryonic disks. The sharp peak in the rotation curve due to a massive central soliton may be observable in ultradiffuse galaxies such as Dragonfly 44 [189]. On the other hand the cuspy density profile $\rho \sim r^{-1}$ expected in CDM-dominated systems should not exist in FDM because the soliton has a homogeneous core.

In contrast to isolated CDM halos, FDM halos of density ρ relax in a manner analogous to gravitating N-body systems, as if they were composed of quasiparticles with mass $\sim\rho(\lambda/2)^3$ (Sec. III C). We suggest that relaxation both adds mass to the central soliton and expels mass to infinity on a time scale given roughly by Eq. (32), but this suggestion needs to be tested by simulations. Relaxation due to FDM quasiparticles or wave packets is probably too weak to affect the disk thickness in the solar neighborhood or to disrupt globular clusters or wide binary stars at or beyond the solar radius, but it may thicken the inner parts of galactic stellar disks and pump energy into stellar bulges. We also suggest that relaxation could produce FDM disks in the central regions of galaxies. The resistance of FDM to compression puts a stringent lower bound on the scale height of a FDM disk; in the solar neighborhood any such disk could not easily have a half-thickness (the distance from the midplane containing half the mass) less than several hundred parsecs or local density greater than $\sim 0.02\, M_\odot\, \mathrm{pc}^{-3}$ (for $m = 10^{-22}$ eV; the thickness and density scale as $m^{-2/3}$ and $m^{2/3}$ respectively).

As noted earlier, dark-matter halos significantly less massive than about $10^7 (m/10^{-22}\ \mathrm{eV})^{-3/2}\ M_\odot$ are not possible in FDM and the limit for subhalos is even stronger because of tunneling of FDM through the tidal radius of the subhalo [Eq. (44)]. Thus the elucidation of the properties of halo substructure within our Galaxy (by studying stellar streams) or along lines of sight through other galaxies (via gravitational lensing) and the study of the dark-matter distribution in low-mass galaxies offer promising tests that could distinguish FDM from CDM.

It has long been a puzzle that the five globular clusters in the Fornax dwarf galaxy have not yet spiraled to the center of that system due to dynamical friction. If the dark matter in Fornax is FDM rather than CDM, our calculations show a substantial increase in the time scale for dynamical friction, and thus FDM essentially solves the problem of the survival of these clusters. Further observational work on the globular cluster systems of other dwarf spheroidal galaxies would be rewarding.

The results discussed so far do not depend directly on the power spectrum of cosmic perturbations, but the expected cutoff of the FDM spectrum at small scales [Eq. (61)] has many further implications. It reduces early galaxy formation below what would have been expected from the CDM model, but this modified formation history is consistent with current observations at $4 \lesssim z \lesssim 10$ [162] and the late reionization, $z \sim 8$, recently reported by *Planck* [163]. There is a substantial reduction in the number of halos expected in the local Universe as compared to CDM for halos below a few times $10^9 (m/10^{-22}\ \mathrm{eV})^{-4/3}\ M_\odot$ but a sufficient number remain to provide for the local dwarf galaxies, which have estimated halo masses of roughly $3 \times 10^9\ M_\odot$ [86]. Thus the too-big-to-fail and missing-satellite problems are addressed directly by FDM, but until our understanding of baryonic physics and feedback is more complete we will not know whether the change in the properties of the dark-matter subhalos implied by FDM is either required or useful.

In summary, the hypothesis that the principal component of the ubiquitous dark matter is an ultralight axion is an attractive and testable alternative to CDM, having no serious inconsistencies with current data if the particle mass $m \gtrsim 10^{-22}$ eV. There are significant and attractive observational consequences if the mass is in the range $1\text{–}10 \times 10^{-22}$ eV. There is tension with observations of the Lyman-α forest, which favor masses $10\text{–}20 \times 10^{-22}$ eV or higher. More sophisticated calculations of reionization and of structure formation in FDM are required to determine whether this variety of constraints is consistent with observations.

ACKNOWLEDGMENTS

We thank Rennan Barkana, Andrei Beloborodov, Tim Brandt, Tom Broadhurst, Justin Khoury, Yuri Levin, Adam

Lidz, David Marsh, Matt McQuinn, Alberto Nicolis, Riccardo Penco, Massimo Pietroni, Hsi-Yu Schive, Uros Seljak, Sergei Sibiriyakov, Pierre Sikivie, David Spergel and Matteo Viel for their comments and insights. This research was supported in part by National Aeronautics and Space Administration Grants No. NNX14AM24G and No. NXX16AB27G, National Science Foundation Grants No. AST-1406166 and No. PHY-1606531, and Department of Energy Grant No. DE-SC0011941.

APPENDIX A: THE QUANTUM VIRIAL THEOREM

In this appendix we derive the quantum-mechanical analog to the classical virial theorem [41].

We begin with the Schrödinger equation

$$i\hbar\frac{\partial\psi}{\partial t} = H\psi = -\frac{\hbar^2}{2m}\nabla^2\psi + m\Phi(\mathbf{r},t)\psi \tag{A1}$$

where H is the Hamiltonian operator; $\Phi(\mathbf{r},t)$ is the gravitational potential; and $m|\psi(\mathbf{r},t)|^2 = \rho(\mathbf{r},t)$, the mass density. The moment of inertia is $I = \frac{1}{2}m\int d\mathbf{r}r^2|\psi|^2$. Then

$$\begin{aligned}\dot{I} &= -\frac{im}{2\hbar}\int d\mathbf{r}r^2(\psi^* H\psi - \psi H\psi^*)\\ &= -\frac{im}{2\hbar}\int d\mathbf{r}\psi^*[r^2, H]\psi\end{aligned} \tag{A2}$$

where $[\cdot,\cdot]$ is the commutator. Since $[r^2,\Phi] = 0$ this simplifies to

$$\dot{I} = \frac{1}{4}i\hbar\int d\mathbf{r}\psi^*[r^2,\nabla^2]\psi. \tag{A3}$$

Similarly,

$$\ddot{I} = \frac{1}{4}\int d\mathbf{r}\psi^*[[r^2,\nabla^2],H]\psi. \tag{A4}$$

Using the result $[[r^2,\nabla^2],H] = -4m(\mathbf{r}\cdot\nabla\Phi) - 4(\hbar^2/m)\nabla^2$ we have

$$\begin{aligned}\ddot{I} &= -\int d\mathbf{r}\psi^*\left(m\psi\mathbf{r}\cdot\nabla\Phi + \frac{\hbar^2}{m}\nabla^2\psi\right)\\ &= -m\int d\mathbf{r}|\psi|^2\mathbf{r}\cdot\nabla\Phi + \frac{\hbar^2}{m}\int d\mathbf{r}|\nabla\psi|^2.\end{aligned} \tag{A5}$$

At this point it is useful to write the wave function in the form $\psi = \sqrt{\rho/m}\exp(i\theta)$ with θ real, and define $\mathbf{v} \equiv \hbar\nabla\theta/m$ [cf. Eq. (22)]. Then

$$\begin{aligned}\ddot{I} &= -\int d\mathbf{r}\rho\mathbf{r}\cdot\nabla\Phi + \int d\mathbf{r}\rho v^2 + \frac{\hbar^2}{m^2}\int d\mathbf{r}|\nabla\sqrt{\rho}|^2\\ &\equiv V + 2K + 2Q.\end{aligned} \tag{A6}$$

This is the quantum virial theorem. The term $K \equiv \frac{1}{2}\int d\mathbf{r}\rho v^2$ is analogous to kinetic energy, although the analogy is exact only in the classical limit. The term Q can be called the quantum energy. If the system is self-gravitating then

$$\Phi(\mathbf{r}) = -G\int\frac{d\mathbf{r}'\rho(\mathbf{r}')}{|\mathbf{r}-\mathbf{r}'|} \tag{A7}$$

so

$$\begin{aligned}V &= -G\int d\mathbf{r}d\mathbf{r}'\frac{\rho(\mathbf{r})\rho(\mathbf{r}')\mathbf{r}\cdot(\mathbf{r}-\mathbf{r}')}{|\mathbf{r}-\mathbf{r}'|^3}\\ &= -\frac{G}{2}\int d\mathbf{r}d\mathbf{r}'\frac{\rho(\mathbf{r})\rho(\mathbf{r}')}{|\mathbf{r}-\mathbf{r}'|} = W\end{aligned} \tag{A8}$$

where W is the total potential energy of the system. The total energy of the system is $K + W + Q$, which is conserved.

In a steady state $\ddot{I} = 0$, and since $K \geq 0$ we have

$$\frac{Q}{|W|} \leq \frac{1}{2} \tag{A9}$$

which sets a lower limit on the particle mass m for an equilibrium system with a given density distribution $\rho(\mathbf{r})$. The limit is saturated ($Q/|W| = \frac{1}{2}$) if the phase of the wave function is position independent so $\nabla\theta = 0$, a condition that is satisfied in the soliton.

APPENDIX B: EIGENSTATES OF THE SCHRÖDINGER-POISSON EQUATION

A useful standard for comparison to theoretical models and simulations of FDM halos is provided by the eigenstates of the time-independent Schrödinger-Poisson equation, which are solutions of the combined equations

$$\begin{aligned}-\frac{\hbar^2}{2m}\nabla^2\psi + m\Phi\psi &= mE\psi,\\ \nabla^2\Phi &= 4\pi Gm|\psi|^2.\end{aligned} \tag{B1}$$

Here $\psi(\mathbf{r})$ and $\Phi(\mathbf{r})$ are the wave function and gravitational potential, and E is the energy per unit mass of the eigenstate. We consider isolated systems so we assume that ψ, Φ approach zero as $|\mathbf{r}| \to \infty$ and that they are regular near the origin. The total mass $M = m\int d\mathbf{r}|\psi|^2$ and it is straightforward to show that $ME = 2W + K + Q$; thus the energy eigenvalue E is *not* the total energy per unit mass of the system. Using the time-independent virial theorem we can show that the energy eigenvalue is related to the potential energy by $W = \frac{2}{3}ME$.

TABLE II. Properties of the lowest eigenstates of the Schrödinger-Poisson equation [Eq. (B4)].

n	ρ_n	ϕ_n	f_n	ϵ_n	w_n
0	0.00440	0.3155	3.9251	0.16277	0.10851
1	0.000180	0.07146	23.562	0.03080	0.02053
2	0.000031	0.03139	60.903	0.012526	0.008351
3	9.400×10^{-6}	0.01772	116.18	0.006747	0.004498
4	3.733×10^{-6}	0.01240	178.60	0.004209	0.002806

We restrict our attention to spherical solutions.[21] Then the wave function can be taken to be real and

$$-\frac{\hbar^2}{2mr^2}\frac{d}{dr}r^2\frac{d\psi}{dr}+m\Phi\psi=mE\psi,$$
$$\frac{1}{r^2}\frac{d}{dr}r^2\frac{d\Phi}{dr}=4\pi Gm\psi^2. \tag{B2}$$

Following other authors [41,57,95,96,190,191] we compute numerically the solutions of these equations, and label the eigenstates $n=0,1,2,\ldots$ in order of increasing energy. The eigenstate labeled by n has n nodal radii at which the density is zero. Because the Schrödinger-Poisson equations admit a scaling invariant, all systems corresponding to a given level n form a one-parameter family that can be specified by the total mass M. Then quantities such as the central density, central potential, half-mass radius, virial velocity, energy eigenvalue, and potential energy can be written

$$\rho_c=\left(\frac{Gm^2}{\hbar^2}\right)^3M^4\rho_n,$$
$$\Phi_c=-\left(\frac{GMm}{\hbar}\right)^2\phi_n,$$
$$r_{1/2}=\frac{\hbar^2}{GMm^2}f_n, \tag{B3}$$

$$v_{\rm vir}=(-W/M)^{1/2}=\frac{GMm}{\hbar}w_n^{1/2},$$
$$E=-\left(\frac{GMm}{\hbar}\right)^2\epsilon_n,$$
$$W=-\frac{G^2M^3m^2}{\hbar^2}w_n. \tag{B4}$$

The dimensionless constants ρ_n, ϕ_n, f_n, ϵ_n, and w_n are given in Table II. Note that $w_n=\frac{2}{3}\epsilon_n$.

We see that the central density is a strongly decreasing function of the level number n so the densest system is the ground state, $n=0$. The ground state is linearly stable but the nth excited state has n spherically symmetric unstable modes which decay to the ground state through the dispersion of probability density to infinity; see Sec. III C and Refs. [56–58]. Thus the ground state, sometimes called a "soliton," is the long-term attractor for any FDM system.

[21] An interesting unsolved problem is whether there are nonspherical solutions of the time-independent Schrödinger-Poisson equation.

APPENDIX C: QUANTUM-MECHANICAL TREATMENT OF THE TIDAL RADIUS

To derive the classical formula for the tidal radius, consider a mass M in a circular orbit of radius a around a point-mass host and work in a rotating Cartesian reference frame that is centered on M, with the z-axis pointing in the same direction as the orbital angular momentum and the x-axis pointing away from the host. Let a and Ω be the orbital radius and angular speed. Then for $r=(x^2+y^2+z^2)^{1/2}\ll a$ the equations of motion for a test particle are [see for example Eq. (8.97) of [55]]

$$\ddot{x}=2\Omega\dot{y}+3\Omega^2x-\frac{GMx}{r^3},$$
$$\ddot{y}=-2\Omega\dot{x}-\frac{GMy}{r^3},$$
$$\ddot{z}=-\Omega^2z-\frac{GMz}{r^3}. \tag{C1}$$

There is an equilibrium solution ($\dot{x}=\dot{y}=\dot{z}=0$) at $x=\pm r_t$, $y=z=0$ where $r_t=(GM/3\Omega^2)^{1/3}$ is the tidal radius. If the host has mass $\mathfrak{M}$ then

$$r_t=a\left(\frac{M}{3\mathfrak{M}}\right)^{1/3}. \tag{C2}$$

We will consider a simplified system, in which the mass M is subjected to a spherically symmetric tidal potential $\Phi_t=-\frac{3}{2}\Omega^2r^2=-\frac{3}{2}G\mathfrak{M}r^2/a^3$. Then we can work in an inertial frame centered on M, in which the equations of motion are

$$\ddot{\mathbf{r}}=-3\Omega^2\mathbf{r}-\frac{GM}{r^3}\mathbf{r}=GM\left(\frac{1}{r_t^3}-\frac{1}{r^3}\right)\mathbf{r}; \tag{C3}$$

these have equilibrium solutions at $r=r_t$ and capture much of the dynamics relevant to tidal disruption.

The Schrödinger-Poisson equation analogous to (C3) is

$$-\frac{\hbar^2}{2m^2r^2}\frac{d}{dr}r^2\frac{d\psi}{dr}+\left(\Phi-\frac{3}{2}\Omega^2r^2\right)\psi=E\psi,$$
$$\frac{1}{r^2}\frac{d}{dr}r^2\frac{d\Phi}{dr}=4\pi Gm\psi^2. \tag{C4}$$

In contrast to the case of particles such as CDM, which can orbit forever if they are inside the tidal radius, FDM is described by the wave equation (C4) which allows matter

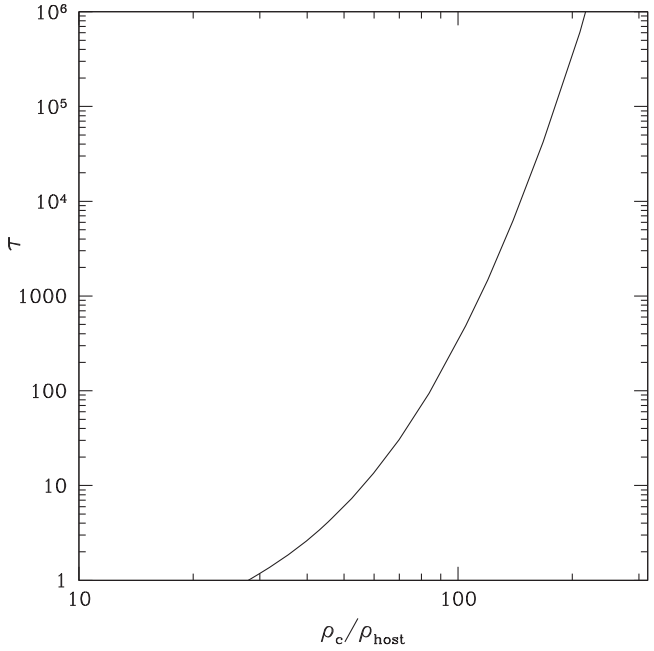

FIG. 1. The lifetime of a stellar system in the ground state of the Schrödinger-Poisson equation when a spherically symmetric tidal field is present. The vertical axis gives the dimensionless lifetime τ in units of the orbital period [Eq. (C7)] and the horizontal axis gives the ratio of the central density to the mean density of the host averaged over the orbital radius.

with $r \ll r_t$ to tunnel through the potential barrier centered on r_t and escape to infinity. Thus all self-gravitating systems in an external tidal field are eventually tidally disrupted. It is worth stressing that by tunneling, we do not mean tunneling in the sense of quantum field theory—classical field theory provides an adequate description of all phenomena discussed in this paper (see comments at the end of Sec. II B).

To determine the disruption time scale, we solve Eqs. (C4) numerically. We impose an outgoing wave boundary condition as $r \to \infty$; using the WKB approximation we can show that this must have the form

$$\psi(r) \to \frac{A}{r^{3/2}} \exp\left(i\frac{\sqrt{3}m\Omega}{2\hbar}r^2\right) \tag{C5}$$

where A is a constant. We impose regular boundary conditions at the origin [$\psi'(r) \sim r$ and $\Phi'(r) \sim r$] and allow the energy eigenvalue E to be complex; then the rate of mass loss is

$$\dot{M} = 2M\mathrm{Im}(E). \tag{C6}$$

We may then define a dimensionless tidal disruption time by

$$\tau \equiv \frac{M\Omega}{2\pi\dot{M}}, \tag{C7}$$

so a system will lose a substantial fraction of its mass due to tides in τ orbits.

In Fig. 1 we show τ as a function of $\rho_c/\rho_{\rm host}$ where ρ_c is the central density of the satellite and $\rho_{\rm host} = 3\mathfrak{M}/(4\pi a^3) = 3\Omega^2/(4\pi G)$ is the mean density of the host galaxy averaged over the distance a to the satellite.

APPENDIX D: QUANTUM-MECHANICAL TREATMENT OF DYNAMICAL FRICTION

The goal of this appendix is to compute the dynamical friction on a point-mass object (the "test object") moving through the FDM superfluid. As the object travels through the fluid, a gravitational wake forms behind it, and the associated overdensity exerts a drag. The wave nature of FDM is expected to suppress the overdensity, reducing the drag.

Let us work in a frame in which the test object, of mass $m_{\rm cl}$, is stationary at the origin, and the dark-matter fluid flows past with a velocity $\mathbf{v}$ and a uniform density ρ in the far past. The dark matter interacts with the object gravitationally, but its self-gravity is ignored [the validity of this approximation is discussed following Eq. (D14)]. This is the classic Coulomb scattering problem. The time-independent Schrödinger equation for the wave function ψ has the solution (e.g., [192])

$$\psi = \mathfrak{N}e^{ikz}M[i\beta, 1, ik(r-z)], \tag{D1}$$

where M is a confluent hypergeometric function. Here z is the coordinate parallel to $\mathbf{v} = v\hat{\mathbf{z}}$, $\hbar k = mv$ is the associated momentum, and r is the radial distance from the point mass. The dimensionless parameter is

$$\beta \equiv \frac{Gm_{\rm cl}m^2}{\hbar^2 k} = \frac{Gm_{\rm cl}m}{\hbar v} = 2\pi\frac{Gm_{\rm cl}}{v^2\lambda}; \tag{D2}$$

apart from the factor of 2π this is the ratio of the characteristic length scale $Gm_{\rm cl}/v^2$ (the impact parameter at which significant deflection of the orbit occurs in the classical limit) to the de Broglie wavelength λ [Eq. (18)]. We are interested in the regime $\beta \ll 1$, whereas the classical description of dynamical friction [55,132] is in the regime $\beta \gg 1$. If we normalize the wave function so that $|\psi|^2$ is the density, then the normalization $\mathfrak{N}$ is determined by the condition that $|\psi|^2 = \rho$ as $-z = r \to \infty$. Up to an unimportant phase,

$$\mathfrak{N} = \sqrt{\rho}e^{\pi\beta/2}|\Gamma(1-i\beta)| \tag{D3}$$

where Γ is the gamma function.

The dynamical friction force is given by a surface integral of the fluid's momentum flux density tensor [Eq. (28)]:

$$\mathbf{F} = F\hat{\mathbf{z}} \quad \text{where } F = -\oint dS_j \Pi_{jz}. \tag{D4}$$

The system is assumed to be in a steady state with no Hubble expansion, so we may set the Hubble constant $H = 0$ and the scale factor $R = 1$. Then using Eq. (27) and the divergence theorem we can show that

$$F = \int d\mathbf{r}\rho \frac{\partial \Phi}{\partial z} \tag{D5}$$

with $\Phi = -GM/r$. Not surprisingly, $-F\hat{\mathbf{z}}$ is the integral of the gravitational force of the object on the surrounding fluid.

We take the surface to be that of a sphere of radius r centered on the test object. We write the frictional force as

$$F = \frac{4\pi G^2 m_{\rm cl}^2 \rho}{v^2} C(\beta, kr). \tag{D6}$$

Then using the solution (D1) and Eqs. (D4) and (D5) respectively, we obtain the two equivalent expressions

$$\begin{aligned} C = {} & \frac{e^{\pi\beta}|\Gamma(1-i\beta)|^2}{2\beta} \int_0^{2kr} dq \left[\left(\frac{kr}{\beta} + 1\right) \right. \\ & \times \left(\frac{q}{kr} - 1\right) |M(i\beta, 1, iq)|^2 + q\,\mathrm{Im}[M(i\beta, 1, iq)^* \\ & \left. \times M(i\beta + 1, 2, iq)] + \beta q |M(i\beta + 1, 2, iq)|^2 \right] \end{aligned} \tag{D7}$$

$$\begin{aligned} = {} & \frac{e^{\pi\beta}|\Gamma(1-i\beta)|^2}{2\beta} \int_0^{2kr} dq |M(i\beta, 1, iq)|^2 \\ & \times \left(\frac{q}{kr} - 2 - \log\frac{q}{2kr}\right). \end{aligned} \tag{D8}$$

The Coulomb scattering problem has infrared divergence ($C \to \infty$ as $r \to \infty$) so we keep r finite; we may think of r as representing either the size of the test object's orbit or the size of its host system, whichever is smaller.

The analogous classical expression[22] can be obtained by determining the momentum flow through a sphere of radius r from hyperbolic Keplerian orbits that are parallel to the z-axis as $z \to -\infty$:

$$C_{\rm cl} = \frac{1+\Lambda}{\Lambda} \tanh^{-1} \frac{\sqrt{\Lambda^2 + 2\Lambda}}{1+\Lambda} - \sqrt{1 + 2/\Lambda} \tag{D9}$$

where

$$\Lambda \equiv \frac{kr}{\beta} = \frac{v^2 r}{G m_{\rm cl}}; \tag{D10}$$

this factor is usually called the "Coulomb logarithm." It is straightforward to verify numerically that Eqs. (D7) and (D8) agree with Eq. (D9) in the limit in which $kr \to \infty$ and $\beta \to \infty$ while $\Lambda = kr/\beta$ is constant.

If the test object is much less massive than the host system in which it resides ($m_{\rm cl} \ll \mathfrak{M}$) then the classical virial theorem[23] implies that $v^2 \sim G\mathfrak{M}/r$ so $\Lambda \sim \mathfrak{M}/m_{\rm cl} \gg 1$. Then

$$C_{\rm cl} = \log 2\Lambda - 1 + \frac{1}{\Lambda}\log 2\Lambda + \mathrm{O}(\Lambda^{-2}). \tag{D11}$$

This formulation differs slightly from the usual treatment due to Chandrasekhar [55,132], who imposed an infrared cutoff by placing an upper bound on the impact parameter rather than the distance from the test object. Thus we should not expect our result to agree exactly with Chandrasekhar's even in the classical limit $kr, \beta \to \infty$ [although both give $C_{\rm Ch} = \log\Lambda + \mathrm{O}(1)$ as $\Lambda \to \infty$]. An exact comparison would require solving a wave packet scattering problem.

If the host system is composed of FDM, the frictional force depends on the dimensionless number $kr = mvr/\hbar$. It is useful to rewrite kr in terms of the half-mass radius $r_{1/2}$ and the virial velocity $v_{\rm vir}$ of the halo. For the ground state, we have from Eq. (B3)

$$kr = f_0 w_0^{1/2} \frac{v}{v_{\rm vir}} \frac{r}{r_{1/2}} = 1.29 \frac{v}{v_{\rm vir}} \frac{r}{r_{1/2}}. \tag{D12}$$

Thus kr is of order unity; then Eq. (D2) implies that $\beta \sim m_{\rm cl}/\mathfrak{M}$ so $\beta \ll 1$ when the test object is much less massive than the host system. A Taylor series expansion of the confluent hypergeometric function gives

$$M(i\beta, 1, iq) = 1 - \beta\,\mathrm{Si}(q) - i\beta\,\mathrm{Cin}(q) + \mathrm{O}(\beta^2), \tag{D13}$$

where $\mathrm{Si}(z) = \int_0^z \sin t\,dt/t$ and $\mathrm{Cin}(z) = \int_0^z (1-\cos t)\,dt/t$ are sine and cosine integrals. Then the integral (D8) is straightforward:

$$C = \mathrm{Cin}(2kr) + \frac{\sin 2kr}{2kr} - 1 + \mathrm{O}(\beta). \tag{D14}$$

For $kr \ll 1$, $C \to \frac{1}{3}(kr)^2$. For $kr \gg 1$, the behavior of C can be derived from Eq. (D7), using results from [193,194]:

$$C = \ln(2kr) - 1 - \mathrm{Re}\Psi(1 + i\beta) + \mathrm{O}(1/kr), \tag{D15}$$

where Ψ is the digamma function, with the following asymptotics: $\mathrm{Re}\Psi(1+i\beta) \to \ln\beta$ for large β, and $-\gamma_E$ for

[22] In this analog we assume that an object of mass $m_{\rm cl}$ travels at speed v through a background of much less massive objects, all at rest, having total density ρ. Of course this analog is unrealistic since the background system would be gravitationally unstable on all scales.

[23] The classical virial theorem applies because the test object behaves classically.

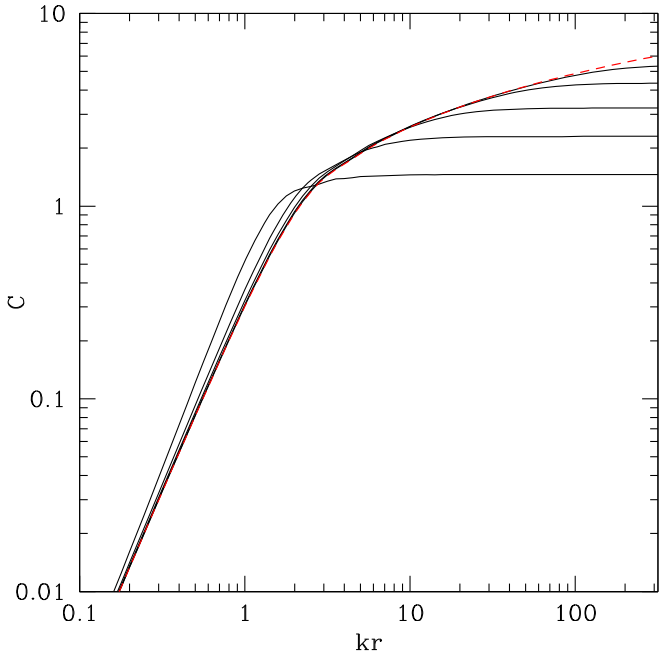

FIG. 2. The dynamical friction force on a test object of mass $m_{\rm cl}$ traveling at speed v through FDM with density ρ is given by Eq. (D6), with the dimensionless function C plotted in this figure. The horizontal axis is kr where $k = mv/\hbar$ is the wave number of the FDM particles in the rest frame of the test object, and r is an upper cutoff to the distance from the test object that approximately represents the smaller of the radius of the orbit and the size of the host system. Each curve is for a fixed value of $\Lambda = v^2 r/Gm_{\rm cl}$, which by the virial theorem is approximately the ratio of the mass of the host to the mass of the test object; from bottom to top $\Lambda = 3, 10, 30, 100, 300$. The dashed red line shows the asymptotic behavior in the limit $\Lambda \to \infty$ [Eq. (D14)].

small β (γ_E is the Euler-Mascheroni constant). This expression has an accuracy of better than 10% down to $kr = 1$, if $\Lambda > 100$.

In deriving these results we have relied on the approximation that the self-gravity of the dark matter can be ignored. This approximation is also used in the classical calculations of dynamical friction, where it is justified because the strongest contribution to the friction comes from scales much smaller than the system size.[24] The approximation is less well justified for FDM since the strongest contribution comes from scales comparable to the size of the solitonic core—according to Eq. (D14) the force is proportional to C which is $\sim(kr)^2$ for $kr \ll 1$.

Figure 2 shows $C(kr/\Lambda, kr)$ [Eq. (D6)] as a function of the dimensionless wave number kr, for $\Lambda = 3, 10, 30, 100, 300$. Recall that the Coulomb logarithm Λ is given by Eq. (D10) and is of order the ratio $\mathfrak{M}/m_{\rm cl}$ of the mass of the host galaxy to the mass of the test object. The solid lines are computed from Eq. (D8) and the dashed red line shows the asymptotic behavior as $\Lambda \to \infty$ [Eq. (D14)]. Figure 2 shows that when $kr \sim 1$, the factor C is also near unity for a wide range of Λ. If on the other hand the test object orbits near the center of the host system then $kr \ll 1$ and $C \to \frac{1}{3}(kr)^2$.

To estimate the time scale for orbital decay, we assume that the test object is on a circular orbit of radius r. Its velocity is given by $v^2 = G\mathfrak{M}(r)/r$ where $\mathfrak{M}(r)$ is the mass of the host system interior to r, and its angular momentum is $L = m_{\rm cl} r v$. Dynamical friction exerts a torque $|F|r$ in the direction opposite to the orbital motion, where F is given by Eq. (D6), so the decay time scale is

$$\tau \equiv \frac{L}{r|F|} = \frac{\mathfrak{M}(r)^{3/2}}{4\pi G^{1/2} m_{\rm cl} \rho r^{3/2} C}. \tag{D16}$$

At orbital radii $r \ll r_{1/2}$, for a solitonic host galaxy, we can further replace C with $\frac{1}{3}(kr)^2 = \frac{1}{3}(mvr/\hbar)^2 = \frac{1}{3}(m/\hbar)^2 G\mathfrak{M}(r) r$, the density ρ with its central value ρ_c from Eq. (B3), and $\mathfrak{M}(r)$ with $\frac{4}{3}\pi\rho_c r^3$. We obtain

$$\tau = \frac{3^{1/2}}{2\pi^{1/2}\rho_0^{1/2} w_0^{1/2} f_0^3} \frac{v_{\rm vir} r_{1/2}^3}{G m_{\rm cl} r} = 0.370 \frac{v_{\rm vir} r_{1/2}^3}{G m_{\rm cl} r}. \tag{D17}$$

APPENDIX E: THE COLLISION OF STREAMS

When two streams of CDM collide, they pass through each other. What should we expect for FDM? On the one hand, it can be thought of as a fluid. Thus multiple-streaming cannot occur; i.e., the density and velocity fields are single-valued. On the other hand, FDM is described by the Schrödinger equation, where the linear superposition of wave functions is permitted (for simplicity, we ignore gravity in this appendix). To illuminate this issue, it is instructive to study two simple analytic solutions.

The free Schrödinger equation in one spatial dimension (ignoring gravity and cosmic expansion) $i\hbar\partial_t\psi = -\hbar^2\partial_x^2\psi/(2m)$ admits a Gaussian superposition of plane waves as a solution:

$$\psi(t,x) \propto \int dk \exp\left[-\frac{1}{2}x_0^2 k^2\right] \exp\left[i\left(kx - \frac{\hbar^2 k^2}{2m} t\right)\right], \tag{E1}$$

where the real number x_0 characterizes the width of the Gaussian. The corresponding density and velocity fields are derived from Eqs. (22):

[24] To see this, note that for $\Lambda \gg 1$ the frictional force varies as $\log 2\Lambda$ according to Eq. (D11). Since $\Lambda \sim r$ according to Eq. (D10) each octave in r contributes equally to the friction. A classical calculation that includes self-gravity is given by [195].

$$\rho(t,x) = \frac{M_{\rm tot}}{\pi^{1/2}x_0(1+\tilde{t}^2)^{1/2}}\exp\left(-\frac{\tilde{x}^2}{1+\tilde{t}^2}\right),$$
$$v(t,x) = \frac{\hbar\tilde{t}\,\tilde{x}}{mx_0(1+\tilde{t}^2)}, \tag{E2}$$

where $M_{\rm tot}$ is the integrated mass, and $\tilde{t}$ and $\tilde{x}$ are the dimensionless time and distance:

$$\tilde{t} \equiv \frac{\hbar t}{mx_0^2}, \qquad \tilde{x} \equiv \frac{x}{x_0}. \tag{E3}$$

This solution describes a flow converging upon the origin at $t<0$, and diverging from it at $t>0$. The density profile is narrowest at $t=0$, with a width of x_0. It is instructive to consider what CDM would predict if one were to initiate ρ and v with values that match the above at some early time $t_{\rm i}$ (<0). In other words, a CDM particle with initial position q has the trajectory

$$x(t) = q + v(t_{\rm i},q)(t-t_{\rm i}). \tag{E4}$$

The velocity is unchanged as the particle free streams and the density follows by mass conservation:

$$\rho(t,x) = \frac{M_{\rm tot}}{\pi^{1/2}x_0}\frac{(1+\tilde{t}_i^{\,2})^{1/2}}{|1+\tilde{t}\tilde{t}_i|}\exp\left[-\frac{(1+\tilde{t}_i^{\,2})}{(1+\tilde{t}\tilde{t}_i)^2}\tilde{x}^2\right],$$
$$v(t,x) = \frac{\hbar\tilde{t}_i\tilde{x}}{mx_0(1+\tilde{t}\tilde{t}_i)}, \tag{E5}$$

where $\tilde{t}_i \equiv \hbar t_i/(mx_0^2)$. Assuming $|\tilde{t}_i| \gg 1$, one can see that the FDM and CDM predictions approximately match for $|\tilde{t}| \gtrsim 1$. For $|\tilde{t}| \lesssim 1$, however, they can be quite different—especially at $\tilde{t} = -1/\tilde{t}_i$ when the CDM density (E5) blows up at the origin, due to the formation of a caustic. In contrast, the FDM density (E2) remains regular at all times.

These differences in behavior between FDM and CDM can be interpreted in two ways. As a fluid, FDM is affected by quantum stress or pressure. The spatial gradient in the density produces pressure that opposes the formation of a density peak that is too narrow; the pressure causes a bounce at the point of collision which eventually erases the peak. Alternatively, one can interpret FDM as a collection of particles, albeit with a long de Broglie wavelength. Wave packets describing these particles do superimpose. The particles stream past each other in both FDM and CDM, but the fuzziness associated with the macroscopic de Broglie wavelength smooths out the caustic in FDM. Both interpretations are valid.

Suppose one observes a collision of two streams at a relative velocity v_0. Based on the above simple example, we expect fuzziness effects to be noticeable for $|x| \lesssim x_0$, $|t| \lesssim t_0$ where

$$x_0 = \frac{\hbar}{mv_0} = 192\ {\rm pc}\,\frac{10^{-22}\ {\rm eV}}{m}\,\frac{100\ {\rm km\,s^{-1}}}{v_0},$$
$$t_0 = \frac{\hbar}{mv_0^2} = 1.87\times10^6\ {\rm yr}\,\frac{10^{-22}\ {\rm eV}}{m}\left(\frac{100\ {\rm km\,s^{-1}}}{v_0}\right)^2. \tag{E6}$$

Thus, for clusters of galaxies, where $v_0 \sim 10^3\ {\rm km\,s^{-1}}$, we do not expect fuzziness to play an important role. Ultimately, gravity should be included in the analysis. When bound objects could form under a collision, the difference between FDM and CDM would no longer be transitory.

For additional insight into the nature of collisions, it is useful to consider self-similar solutions. The free Schrödinger equation has the symmetry $x \to \lambda x$, $t \to \lambda^2 t$. It is thus natural to look for a solution which is a function of $x/\sqrt{t}$ alone:

$$\psi(t,x) = \frac{\mathcal{A}}{\sqrt{2\pi}}e^{-i\pi/4}\int_{x\sqrt{m/\hbar t}}^{\infty} e^{i\xi^2/2}d\xi + \mathcal{B}, \tag{E7}$$

where $\mathcal{A}$ and $\mathcal{B}$ are constants. (For $t<0$, we choose $x\sqrt{m/\hbar t} = ix\sqrt{m/\hbar|t|}$.) The solution has simple spatial asymptotics:

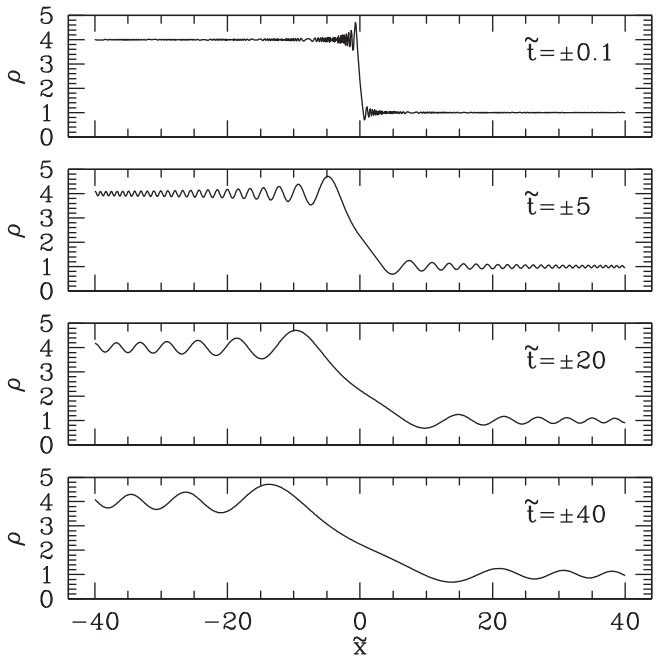

FIG. 3. Density evolution in a self-similar FDM solution, according to Eq. (E9). The dimensionless time $\tilde{t}$ and distance $\tilde{x}$ are defined in Eq. (E3), where x_0 is an arbitrary length scale. The overall normalization of the density ρ is also arbitrary. With the choice $\mathcal{A} = \mathcal{B}$ made here, the ratio of the asymptotic density at $x \to \pm\infty$ is $(\mathcal{A}+\mathcal{B})^2/\mathcal{B}^2 = 4$.

$$\psi(t, x \to -\infty) = \mathcal{A} + \mathcal{B}, \qquad \psi(t, x \to \infty) = \mathcal{B}. \tag{E8}$$

We choose $\mathcal{A}$ and $\mathcal{B}$ to be real. The asymptotic behavior of the density $\rho = |\psi|^2$ is $\rho \to (\mathcal{A}+\mathcal{B})^2$ as $x \to -\infty$ and $\rho \to \mathcal{B}^2$ as $x \to \infty$. There is thus a jump in density. Moreover, the jump becomes increasingly sharp as $t \to 0$. This resembles what one expects for shock formation in a normal fluid. Let us write out ψ more explicitly as

$$\psi(t,x) = \frac{\mathcal{A}}{2} + \mathcal{B} - \frac{\mathcal{A}}{2}(1 \mp i)\mathcal{C}\left(x\sqrt{\frac{m}{\pi\hbar|t|}}\right) - \frac{\mathcal{A}}{2}(1 \pm i)\mathcal{S}\left(x\sqrt{\frac{m}{\pi\hbar|t|}}\right), \tag{E9}$$

where the upper/lower sign is for a positive/negative t. The functions $\mathcal{C}$ and $\mathcal{S}$ are the Fresnel integrals, defined by

$$\mathcal{C}(\theta) = \int_0^\theta \cos\left(\frac{1}{2}\pi\xi^2\right)d\xi, \qquad \mathcal{S}(\theta) = \int_0^\theta \sin\left(\frac{1}{2}\pi\xi^2\right)d\xi. \tag{E10}$$

The implied density $\rho = |\psi|^2$ is depicted in Fig. 3.

The resemblance to a shock (in its rest frame) is superficial. The evolution in the case of FDM is time-reversal symmetric, whereas there is an irreversible entropy production in a normal shock. From a fluid perspective, the quantum pressure of FDM reacts against the steepening density profile around $x = 0$, ultimately causing a bounce that reverses the evolution. From a particle perspective, the two colliding streams go past each other after $t = 0$, much as CDM would, thereby smoothing out the jump in density around $x = 0$. The difference from CDM is the absence of caustics where density formally diverges. The FDM density profile has characteristic oscillations on the scale $x \sim \sqrt{\hbar|t|/m}$.

[1] P. A. R. Ade *et al.* (Planck Collaboration), Planck 2015 results. XIII. Cosmological parameters, Astron. Astrophys. **594**, A13 (2016).
[2] J. Dubinski and R. G. Carlberg, The structure of cold dark matter halos, Astrophys. J. **378**, 496 (1991).
[3] J. F. Navarro, C. S. Frenk, and S. D. M. White, A universal density profile from hierarchical clustering, Astrophys. J. **490**, 493 (1997).
[4] D. H. Weinberg, J. S. Bullock, F. Governato, R. Kuzio de Naray, and A. H. G. Peter, Cold dark matter: Controversies on small scales, Proc. Natl. Acad. Sci. U.S.A. **112**, 12249 (2015).
[5] M. Viel, J. Lesgourgues, M. G. Haehnelt, S. Matarrese, and A. Riotto, Constraining warm dark matter candidates including sterile neutrinos and light gravitinos with WMAP and the Lyman-α forest, Phys. Rev. D **71**, 063534 (2005).
[6] P. Colín, V. Avila-Reese, and O. Valenzuela, Substructure and halo density profiles in a warm dark matter cosmology, Astrophys. J. **542**, 622 (2000).
[7] P. Bode, J. P. Ostriker, and N. Turok, Halo formation in warm dark matter models, Astrophys. J. **556**, 93 (2001).
[8] S. Tremaine and J. E. Gunn, Dynamical Role of Light Neutral Leptons in Cosmology, Phys. Rev. Lett. **42**, 407 (1979).
[9] M. S. Turner, Coherent scalar field oscillations in an expanding universe, Phys. Rev. D **28**, 1243 (1983).
[10] W. H. Press, B. S. Ryden, and D. N. Spergel, Single Mechanism for Generating Large-Scale Structure and Providing Dark Missing Matter, Phys. Rev. Lett. **64**, 1084 (1990).
[11] S.-J. Sin, Late time cosmological phase transition and galactic halo as Bose liquid, Phys. Rev. D **50**, 3650 (1994).
[12] W. Hu, R. Barkana, and A. Gruzinov, Cold and Fuzzy Dark Matter, Phys. Rev. Lett. **85**, 1158 (2000).
[13] J. Goodman, Repulsive dark matter, New Astron. **5**, 103 (2000).
[14] P. J. E. Peebles, Fluid dark matter, Astrophys. J. **534**, L127 (2000).
[15] L. Amendola and R. Barbieri, Dark matter from an ultra-light pseudo-Goldstone-boson, Phys. Lett. B **642**, 192 (2006).
[16] H.-Y. Schive, T. Chiueh, and T. Broadhurst, Cosmic structure as the quantum interference of a coherent dark wave, Nat. Phys. **10**, 496 (2014).
[17] D. J. E. Marsh, Axion cosmology, Phys. Rep. **643**, 1 (2016).
[18] R. Hlozek, D. Grin, D. J. E. Marsh, and P. G. Ferreira, A search for ultralight axions using precision cosmological data, Phys. Rev. D **91**, 103512 (2015).
[19] M. Viel, G. D. Becker, J. S. Bolton, and M. G. Haehnelt, Warm dark matter as a solution to the small scale crisis: New constraints from high redshift Lyman-α forest data, Phys. Rev. D **88**, 043502 (2013).
[20] P. Sikivie, Experimental Tests of the Invisible Axion, Phys. Rev. Lett. **51**, 1415 (1983); Erratum, Phys. Rev. Lett.**52**, 695(E) (1984).
[21] J. Hoskins, J. Hwang, C. Martin, P. Sikivie, N. S. Sullivan, D. B. Tanner, M. Hotz, L. J Rosenberg, G. Rybka, A. Wagner, S. J. Asztalos, G. Carosi, C. Hagmann, D. Kinion, K. van Bibber, R. Bradley, and J. Clarke, A search for non-virialized axionic dark matter, Phys. Rev. D **84**, 121302 (2011).

[22] J. Ruz, J. K. Vogel, and M. J. Pivovaroff (CAST Collaboration), Recent constraints on axion-photon and axion-electron coupling with the CAST experiment, Phys. Procedia **61**, 153 (2015).
[23] A. Arvanitaki, S. Dimopoulos, S. Dubovsky, N. Kaloper, and J. March-Russell, String axiverse, Phys. Rev. D **81**, 123530 (2010).
[24] K. Choi and J. E. Kim, Compactification and axions in $E(8) \times E(8)$-prime superstring models, Phys. Lett. B **165B**, 71 (1985).
[25] T. Banks, M. Dine, P. J. Fox, and E. Gorbatov, On the possibility of large axion decay constants, J. Cosmol. Astropart. Phys. 06 (2003) 001.
[26] P. Svrcek and E. Witten, Axions in string theory, J. High Energy Phys. 06 (2006) 051.
[27] N. Arkani-Hamed, A. Gupta, D. E. Kaplan, N. Weiner, and T. Zorawski, Simply unnatural supersymmetry, arXiv: 1212.6971.
[28] P. Svrcek, Cosmological constant and axions in string theory, arXiv:hep-th/0607086.
[29] J. Preskill, M. B. Wise, and F. Wilczek, Cosmology of the invisible axion, Phys. Lett. B **120B**, 127 (1983).
[30] L. F. Abbott and P. Sikivie, A cosmological bound on the invisible axion, Phys. Lett. B **120B**, 133 (1983).
[31] M. Dine and W. Fischler, The not so harmless axion, Phys. Lett. B **120B**, 137 (1983).
[32] J. E. Kim and D. J. E. Marsh, An ultralight pseudoscalar boson, Phys. Rev. D **93**, 025027 (2016).
[33] D. J. E. Marsh, D. Grin, R. Hlozek, and P. G. Ferreira, Tensor Interpretation of BICEP2 Results Severely Constrains Axion Dark Matter, Phys. Rev. Lett. **113**, 011801 (2014).
[34] P. W. Graham and S. Rajendran, New observables for direct detection of axion dark matter, Phys. Rev. D **88**, 035023 (2013).
[35] A. Khmelnitsky and V. Rubakov, Pulsar timing signal from ultralight scalar dark matter, J. Cosmol. Astropart. Phys. 02 (2014) 019.
[36] A. H. Guth, M. P. Hertzberg, and C. Prescod-Weinstein, Do dark matter axions form a condensate with long-range correlation?, Phys. Rev. D **92**, 103513 (2015).
[37] Lawrence M. Widrow and Nick Kaiser, Using the Schrodinger equation to simulate collisionless matter, Astrophys. J. **416**, L71 (1993).
[38] Cora Uhlemann, Michael Kopp, and Thomas Haugg, Schrödinger method as N-body double and UV completion of dust, Phys. Rev. D **90**, 023517 (2014).
[39] R. P. Feynman, R. B. Leighton, and M. Sands, *The Feynman Lectures on Physics* (Addison Wesley Longman, Reading, MA, 1963).
[40] E. A. Spiegel, Fluid dynamical form of the linear and nonlinear Schrödinger equations, Physica D (Amsterdam) **1D**, 236 (1980).
[41] P.-H. Chavanis, Mass-radius relation of Newtonian self-gravitating Bose-Einstein condensates with short-range interactions. I. Analytical results, Phys. Rev. D **84**, 043531 (2011).
[42] A. Suárez and T. Matos, Structure formation with scalar-field dark matter: The fluid approach, Mon. Not. R. Astron. Soc. **416**, 87 (2011).
[43] C. Uhlemann, M. Kopp, and T. Haugg, Schrödinger method as N-body double and UV completion of dust, Phys. Rev. D **90**, 023517 (2014).
[44] D. J. E. Marsh, Nonlinear hydrodynamics of axion dark matter: Relative velocity effects and quantum forces, Phys. Rev. D **91**, 123520 (2015).
[45] B. Schwabe, J. C. Niemeyer, and J. F. Engels, Simulations of solitonic core mergers in ultralight axion dark matter cosmologies, Phys. Rev. D **94**, 043513 (2016).
[46] P. Mocz and S. Succi, Numerical solution of the nonlinear Schrödinger equation using smoothed-particle hydrodynamics, Phys. Rev. E **91**, 053304 (2015).
[47] J. Eby, P. Suranyi, and L. C. R. Wijewardhana, The lifetime of axion stars, Mod. Phys. Lett. A **31**, 1650090 (2016).
[48] A. W. McConnachie, The observed properties of dwarf galaxies in and around the Local Group, Astron. J. **144**, 4 (2012).
[49] S.-R. Chen, H.-Y. Schive, and T. Chiueh, Jeans analysis for dwarf spheroidal galaxies in wave dark matter, arXiv: 1606.09030.
[50] D. J. E. Marsh and A.-R. Pop, Axion dark matter, solitons and the cusp–core problem, Mon. Not. R. Astron. Soc. **451**, 2479 (2015).
[51] E. Calabrese and D. N. Spergel, Ultra-light dark matter in ultra-faint dwarf galaxies, Mon. Not. R. Astron. Soc. **460**, 4397 (2016).
[52] A. X. Gonzáles-Morales, D. J. E. Marsh, J. Peñarrubia, and L. Ureña-López, Unbiased constraints on ultralight axion mass from dwarf spheroidal galaxies, arXiv:1609.05856.
[53] H.-Y. Schive, M.-H. Liao, T.-P. Woo, S.-K. Wong, T. Chiueh, T. Broadhurst, and W.-Y. Pauchy Hwang, Understanding the Core-Halo Relation of Quantum Wave Dark Matter from 3D Simulations, Phys. Rev. Lett. **113**, 261302 (2014).
[54] J. Veltmaat and J. C. Niemeyer, Cosmological particle-in-cell simulations with ultra-light axion dark matter, arXiv:1608.00802.
[55] J. Binney and S. Tremaine, *Galactic Dynamics* 2nd ed. (Princeton University Press, Princeton, NJ, 2008).
[56] E. Seidel and W.-M. Suen, Formation of Solitonic Stars through Gravitational Cooling, Phys. Rev. Lett. **72**, 2516 (1994).
[57] R. Harrison, I. Moroz, and K. P. Tod, A numerical study of the Schrödinger-Newton equations, Nonlinearity **16**, 101 (2003).
[58] F. S. Guzman and L. A. Urena-Lopez, Gravitational cooling of self-gravitating Bose condensates, Astrophys. J. **645**, 814 (2006).
[59] C. G. Lacey and J. P. Ostriker, Massive black holes in galactic halos?, Astrophys. J. **299**, 633 (1985).
[60] B. J. Carr and C. G. Lacey, Dark clusters in galactic halos?, Astrophys. J. **316**, 23 (1987).
[61] M. C. Begelman, R. D. Blandford, and M. J. Rees, Massive black hole binaries in active galactic nuclei, Nature (London) **287**, 307 (1980).
[62] Q. Yu, Evolution of massive binary black holes, Mon. Not. R. Astron. Soc. **331**, 935 (2002).
[63] J. F. Navarro, V. R. Eke, and C. S. Frenk, The cores of dwarf galaxy halos, Mon. Not. R. Astron. Soc. **283**, L72 (1996).

[64] A. El-Zant, I. Shlosman, and Y. Hoffman, Dark halos: The flattening of the density cusp by dynamical friction, Astrophys. J. **560**, 636 (2001).
[65] O. Y. Gnedin and H. Zhao, Maximum feedback and dark matter profiles of dwarf galaxies, Mon. Not. R. Astron. Soc. **333**, 299 (2002).
[66] J. I. Read and G. Gilmore, Mass loss from dwarf spheroidal galaxies: The origins of shallow dark matter cores and exponential surface brightness profiles, Mon. Not. R. Astron. Soc. **356**, 107 (2005).
[67] C. Tonini, A. Lapi, and P. Salucci, Angular momentum transfer in dark matter halos: Erasing the cusp, Astrophys. J. **649**, 591 (2006).
[68] S. Mashchenko, J. Wadsley, and H. M. P. Couchman, Stellar feedback in dwarf galaxy formation, Science **319**, 174 (2008).
[69] E. Romano-Diaz, I. Shlosman, Y. Hoffman, and C. Heller, Erasing dark matter cusps in cosmological galactic halos with baryons, Astrophys. J. **685**, L105 (2008).
[70] T. Goerdt, J. I. Read, B. Moore, and J. Stadel, Core creation in galaxies and haloes via sinking massive objects, Astrophys. J. **725**, 1707 (2010).
[71] F. Governato, C. Brook, L. Mayer, A. Brooks, G. Rhee, J. Wadsley, P. Jonsson, B. Willman, G. Stinson, T. Quinn, and P. Madau, Bulgeless dwarf galaxies and dark matter cores from supernova-driven outflows, Nature (London) **463**, 203 (2010).
[72] D. Cole, W. Dehnen, and M. Wilkinson, Weakening dark-matter cusps by clumpy baryonic infall, Mon. Not. R. Astron. Soc. **416**, 1118 (2011).
[73] A. Pontzen and F. Governato, How supernova feedback turns dark matter cusps into cores, Mon. Not. R. Astron. Soc. **421**, 3464 (2012).
[74] J. Kleyna, M. I. Wilkinson, N. W. Evans, G. Gilmore, and C. Frayn, Dark matter in dwarf spheroidals—II. Observations and modelling of Draco, Mon. Not. R. Astron. Soc. **330**, 792 (2002).
[75] T. Goerdt, B. Moore, J. I. Read, J. Stadel, and M. Zemp, Does the Fornax dwarf spheroidal have a central cusp or core?, Mon. Not. R. Astron. Soc. **368**, 1073 (2006).
[76] X. Wu, The mass distribution of dwarf spheroidal galaxies from stellar kinematics: Draco, Ursa Minor and Fornax, arXiv:astro-ph/0702233.
[77] G. Battaglia, A. Helmi, E. Tolstoy, M. Irwin, V. Hill, and P. Jablonka, The kinematic status and mass content of the Sculptor dwarf spheroidal galaxy, Astrophys. J. **681**, L13 (2008).
[78] M. G. Walker, M. Mateo, E. W. Olszewski, J. Penarrubia, N. W. Evans, and G. Gilmore, A universal mass profile for dwarf spheroidal galaxies, Astrophys. J. **704**, 1274 (2009); Erratum, Astrophys. J.**710**, 886(E) (2010).
[79] L. E. Strigari, C. S. Frenk, and S. D. M. White, Kinematics of Milky Way satellites in a lambda cold dark matter universe, Mon. Not. R. Astron. Soc. **408**, 2364 (2010).
[80] M. G. Walker and J. Penarrubia, A method for measuring (slopes of) the mass profiles of dwarf spheroidal galaxies, Astrophys. J. **742**, 20 (2011).
[81] N. C. Amorisco and N. W. Evans, Dark matter cores and cusps: The case of multiple stellar populations in dwarf spheroidals, Mon. Not. R. Astron. Soc. **419**, 184 (2012).
[82] N. C. Amorisco, A. Agnello, and N. W. Evans, The core size of the Fornax dwarf spheroidal, Mon. Not. R. Astron. Soc. **429**, L89 (2013).
[83] M. A. Breddels and A. Helmi, Model comparison of the dark matter profiles of Fornax, Sculptor, Carina and Sextans, Astron. Astrophys. **558**, A35 (2013).
[84] J. R. Jardel and K. Gebhardt, Variations in a universal dark matter profile for dwarf spheroidals, Astrophys. J. **775**, L30 (2013).
[85] L. E. Strigari, C. S. Frenk, and S. D. M. White, Dynamical models for the Sculptor dwarf spheroidal in a lambda CDM universe, arXiv:1406.6079.
[86] A. Fattahi, J. F. Navarro, T. Sawala, C. S. Frenk, L. V. Sales, K. Oman, M. Schaller, and J. Wang, The cold dark matter content of Galactic dwarf spheroidals: No cores, no failures, no problem, arXiv:1607.06479.
[87] W. J. G. de Blok, S. S. McGaugh, A. Bosma, and V. C. Rubin, Mass density profiles of LSB galaxies, Astrophys. J. **552**, L23 (2001).
[88] W. J. G. de Blok, Halo mass profiles and low surface brightness galaxies rotation curves, Astrophys. J. **634**, 227 (2005).
[89] S.-H. Oh, W. J. G. de Blok, F. Walter, E. Brinks, and R. C. Kennicutt, High-resolution dark matter density profiles of THINGS dwarf galaxies: Correcting for non-circular motions, Astron. J. **136**, 2761 (2008).
[90] W. J. G. de Blok, The core-cusp problem, Adv. Astron. **2010**, 789293 (2010).
[91] M. Khlopov, B. A. Malomed, and Ia. B. Zeldovich, Gravitational instability of scalar fields and formation of primordial black holes, Mon. Not. R. Astron. Soc. **215**, 575 (1985).
[92] M. Bianchi, D. Grasso, and R. Ruffini, Jeans mass of a cosmological coherent scalar field, Astron. Astrophys. **231**, 301 (1990).
[93] M. C. Johnson and M. Kamionkowski, Dynamical and gravitational instability of an oscillating-field dark energy and dark matter, Phys. Rev. D **78**, 063010 (2008).
[94] J.-W. Lee and S. Lim, Minimum mass of galaxies from BEC or scalar field dark matter, J. Cosmol. Astropart. Phys. 1 (2010) 007.
[95] D. J. Kaup, Klein–Gordon geon, Phys. Rev. **172**, 1331 (1968).
[96] R. Ruffini and S. Bonazzola, Systems of self-gravitating particles in general relativity and the concept of an equation of state, Phys. Rev. **187**, 1767 (1969).
[97] T. Helfer, D. J. E. Marsh, K. Clough, M. Fairbairn, E. A. Lim, and R. Becerril, Black hole formation from axion stars, arXiv:1609.04724.
[98] J. Eby, C. Kouvaris, N. G. Nielsen, and L. C. R. Wijewardhana, Boson stars from self-interacting dark matter, J. High Energy Phys. 02 (2016) 028.
[99] J. Eby, P. Suranyi, and L. C. R. Wijewardhana, The lifetime of axion stars, Mod. Phys. Lett. A **31**, 1650090 (2016).
[100] A. A. Klypin, A. V. Kravtsov, O. Valenzuela, and F. Prada, Where are the missing Galactic satellites?, Astrophys. J. **522**, 82 (1999).
[101] B. Moore, S. Ghigna, F. Governato, G. Lake, T. R. Quinn, J. Stadel, and P. Tozzi, Dark matter substructure within galactic halos, Astrophys. J. **524**, L19 (1999).

[102] A. R. Wetzel, P. F. Hopkins, J.-H. Kim, C.-A. Faucher-Giguère, D. Kereš, and E. Quataert, Reconciling dwarf galaxies with ΛCDM cosmology: Simulating a realistic population of satellites around a Milky Way–mass galaxy, Astrophys. J. Lett. **827**, L23 (2016).
[103] A. M. Nierenberg, T. Treu, N. Menci, Y. Lu, P. Torrey, and M. Vogelsberger, The missing satellite problem in 3D, arXiv:1603.01614.
[104] S. Mao and P. Schneider, Evidence for substructure in lens galaxies?, Mon. Not. R. Astron. Soc. **295**, 587 (1998).
[105] R. Li, C. S. Frenk, S. Cole, L. Gao, S. Bose, and W. A. Hellwing, Constraints on the identity of the dark matter from strong gravitational lenses, Mon. Not. R. Astron. Soc. **460**, 363 (2016).
[106] Y. D. Hezaveh, N. Dalal, D. P. Marrone, Y.-Y. Mao, W. Morningstar, D. Wen, R. D. Blandford, J. E. Carlstrom, C. D. Fassnacht, G. P. Holder, A. Kemball, P. J. Marshall, N. Murray, L. P. Levasseur, J. D. Vieira, and R. H. Wechsler, Detection of lensing substructure using ALMA observations of the dusty galaxy SDP.81, Astrophys. J. **823**, 37 (2016).
[107] J. I. Read, M. I. Wilkinson, N. W. Evans, G. Gilmore, and J. T. Kleyna, The importance of tides for the Local Group dwarf spheroidals, Mon. Not. R. Astron. Soc. **367**, 387 (2006).
[108] M. Boylan-Kolchin, J. S. Bullock, and M. Kaplinghat, Too big to fail? The puzzling darkness of massive Milky Way subhaloes, Mon. Not. R. Astron. Soc. **415**, L40 (2011).
[109] D. J. E. Marsh and J. Silk, A model for halo formation with axion mixed dark matter, Mon. Not. R. Astron. Soc. **437**, 2652 (2014).
[110] A. Renzini, Origin of multiple stellar populations in globular clusters and their helium enrichment, Mon. Not. R. Astron. Soc. **391**, 354 (2008).
[111] P. J. E. Peebles and R. H. Dicke, Origin of the globular star clusters, Astrophys. J. **154**, 891 (1968).
[112] P. J. E. Peebles, Dark matter and the origin of galaxies and globular star clusters, Astrophys. J. **277**, 470 (1984).
[113] C. Conroy, A. Loeb, and D. N. Spergel, Evidence against dark matter halos surrounding the globular clusters MGC1 and NGC 2419, Astrophys. J. **741**, 72 (2011).
[114] R. Ibata, C. Nipoti, A. Sollima, M. Bellazzini, S. C. Chapman, and E. Dalessandro, Do globular clusters possess dark matter haloes? A case study in NGC 2419, Mon. Not. R. Astron. Soc. **428**, 3648 (2013).
[115] F. I. Diakogiannis, G. F. Lewis, and R. A. Ibata, Dynamical modelling of NGC 6809: Selecting the best model using Bayesian inference, Mon. Not. R. Astron. Soc. **437**, 3172 (2014).
[116] K. V. Johnston and R. G. Carlberg, Tidal debris as a dark matter probe, in *Astrophysics and Space Science Library*, edited by H. J. Newberg and J. L. Carlin (Springer International Publishing, Switzerland, 2016), Vol. 420, p. 169.
[117] S. Chandrasekhar, On the stability of binary systems, Astrophys. J. **99**, 54 (1944).
[118] J. N. Bahcall, P. Hut, and S. Tremaine, Maximum mass of objects that constitute unseen disk material, Astrophys. J. **290**, 15 (1985).
[119] K. V. Johnston, D. N. Spergel, and C. Haydn, How lumpy is the Milky Way's dark matter halo?, Astrophys. J. **570**, 656 (2002).
[120] J. H. Yoon, K. V. Johnston, and D. W. Hogg, Clumpy streams from clumpy halos: Detecting missing satellites with cold stellar structures, Astrophys. J. **731**, 58 (2011).
[121] J. L. Sanders, J. Bovy, and D. Erkal, Dynamics of stream-subhalo interactions, Mon. Not. R. Astron. Soc. **457**, 3817 (2016).
[122] D. Erkal, V. Belokurov, J. Bovy, and J. L. Sanders, The number and size of subhalo-induced gaps in stellar streams, Mon. Not. R. Astron. Soc. **463**, 102 (2016).
[123] R. G. Carlberg, Star stream folding by dark galactic subhalos, Astrophys. J. **705**, L223 (2009).
[124] D. Erkal and V. Belokurov, Forensics of subhalo-stream encounters: The three phases of gap growth, Mon. Not. R. Astron. Soc. **450**, 1136 (2015).
[125] N. C. Amorisco, F. A. Gòmez, S. Vegetti, and S. D. M. White, Gaps in globular cluster streams: Giant molecular clouds can cause them too, arXiv:1606.02715.
[126] J. Diemand, M. Kuhlen, and P. Madau, Dark matter substructure and gamma-ray annihilation in the Milky Way halo, Astrophys. J. **657**, 262 (2007).
[127] W. Ngan, R. G. Carlberg, B. Bozek, R. F. G. Wyse, A. S. Szalay, and P. Madau, Dispersal of tidal debris in a Milky-Way-sized dark matter halo, Astrophys. J. **818**, 194 (2016).
[128] J. Bovy and H.-W. Rix, A direct dynamical measurement of the Milky Way's disk surface density profile, disk scale length, and dark matter profile at kpc $\lesssim R \lesssim 9$ kpc, Astrophys. J. **779**, 115 (2013).
[129] J. Holmberg and C. Flynn, The local density of matter mapped by Hipparcos, Mon. Not. R. Astron. Soc. **313**, 209 (2000).
[130] J. Bovy and S. Tremaine, On the local dark matter density, Astrophys. J. **756**, 89 (2012).
[131] L. Randall and M. Reece, Dark Matter as a Trigger for Periodic Comet Impacts, Phys. Rev. Lett. **112**, 161301 (2014).
[132] S. Chandrasekhar, Dynamical friction. I. General considerations: The coefficient of dynamical friction, Astrophys. J. **97**, 255 (1943).
[133] S. D. Tremaine, The formation of the nuclei of galaxies. II. The Local Group, Astrophys. J. **203**, 345 (1976).
[134] J. M. Lotz, R. Telford, H. C. Ferguson, B. W. Miller, M. Stiavelli, and J. Mack, Dynamical friction in dE globular cluster systems, Astrophys. J. **552**, 572 (2001).
[135] K. S. Oh, D. N. C. Lin, and H. B. Richer, Globular clusters in the Fornax dwarf spheroidal galaxy, Astrophys. J. **531**, 727 (2000).
[136] S. Inoue, Corrective effect of many-body interactions in dynamical friction, Mon. Not. R. Astron. Soc. **416**, 1181 (2011).
[137] D. R. Cole, W. Dehnen, J. I. Read, and M. I. Wilkinson, The mass distribution of the Fornax dSph: Constraints from its globular cluster distribution, Mon. Not. R. Astron. Soc. **426**, 601 (2012).
[138] S. Tremaine and M. D. Weinberg, Dynamical friction in spherical systems, Mon. Not. R. Astron. Soc. **209**, 729 (1984).

[139] J. I. Read, T. Goerdt, B. Moore, A. P. Pontzen, J. Stadel, and G. Lake, Dynamical friction in constant density cores: A failure of the Chandrasekhar formula, Mon. Not. R. Astron. Soc. **373**, 1451 (2006).
[140] C. S. Kochanek and M. J. White, A quantitative study of interacting dark matter in halos, Astrophys. J. **543**, 514 (2000).
[141] J. J. Dalcanton and C. J. Hogan, Halo cores and phase space densities: Observational constraints on dark matter physics and structure formation, Astrophys. J. **561**, 35 (2001).
[142] F. J. Sanchez-Salcedo, J. Reyes-Iturbide, and X. Hernandez, An extensive study of dynamical friction in dwarf galaxies: The role of stars, dark matter, halo profiles and MOND, Mon. Not. R. Astron. Soc. **370**, 1829 (2006).
[143] F. Villaescusa-Navarro and N. Dalal, Cores and cusps in warm dark matter halos, J. Cosmol. Astropart. Phys. 03 (2011) 024.
[144] A. V. Maccio, S. Paduroiu, D. Anderhalden, A. Schneider, and B. Moore, Cores in warm dark matter haloes: A Catch 22 problem, Mon. Not. R. Astron. Soc. **424**, 1105 (2012).
[145] L. Berezhiani and J. Khoury, Theory of dark matter superfluidity, Phys. Rev. D **92**, 103510 (2015).
[146] V. Lora, J. Magana, A. Bernal, F. J. Sanchez-Salcedo, and E. K. Grebel, On the mass of ultra-light bosonic dark matter from galactic dynamics, J. Cosmol. Astropart. Phys. 02 (2012) 011.
[147] J. A. Sellwood, Galaxy models with live halos, Astron. Astrophys. **89**, 296 (1980).
[148] M. D. Weinberg, Evolution of barred galaxies by dynamical friction, Mon. Not. R. Astron. Soc. **213**, 451 (1985).
[149] V. P. Debattista and J. A. Sellwood, Constraints from dynamical friction on the dark matter content of barred galaxies, Astrophys. J. **543**, 704 (2000).
[150] M. D. Weinberg and N. Katz, Bar-driven dark halo evolution: A resolution of the cusp-core controversy, Astrophys. J. **580**, 627 (2002).
[151] J. Dubinski, I. Berentzen, and I. Shlosman, Anatomy of the bar instability in cuspy dark matter halos, Astrophys. J. **697**, 293 (2009).
[152] E. Athanassoula, Bar slowdown and the distribution of dark matter in barred galaxies, Mon. Not. R. Astron. Soc. **438**, L81 (2014).
[153] J. A. Sellwood, Secular evolution in disk galaxies, Rev. Mod. Phys. **86**, 1 (2014).
[154] J. A. L. Aguerri *et al.*, Bar pattern speeds in CALIFA galaxies: I. Fast bars across the Hubble sequence, Astron. Astrophys. **576**, A102 (2015).
[155] M. S. Petersen, M. D. Weinberg, and N. Katz, Dark matter trapping by stellar bars: The shadow bar, arXiv:1602.04826.
[156] K. Gebhardt, J. Adams, D. Richstone, T. R. Lauer, S. M. Faber, K. Gültekin, J. Murphy, and S. Tremaine, The black hole mass in M87 from Gemini/NIFS adaptive optics observations, Astrophys. J. **729**, 119 (2011).
[157] N. J. McConnell, C.-P. Ma, K. Gebhardt, S. A. Wright, J. D. Murphy, T. R. Lauer, J. R. Graham, and D. O. Richstone, Two ten-billion-solar-mass black holes at the centres of giant elliptical galaxies, Nature (London) **480**, 215 (2011).
[158] J. Kormendy and L. C. Ho, Coevolution (or not) of supermassive black holes and host galaxies, Annu. Rev. Astron. Astrophys. **51**, 511 (2013).
[159] B. Binggeli, G. A. Tammann, and A. Sandage, Studies of the Virgo cluster. VI. Morphological and kinematical structure of the Virgo cluster, Astron. J. **94**, 251 (1987).
[160] M. Fitchett and R. Webster, Substructure in the Coma cluster, Astrophys. J. **317**, 653 (1987).
[161] W. G. Unruh, Absorption cross section of small black holes, Phys. Rev. D **14**, 3251 (1976).
[162] H.-Y. Schive, T. Chiueh, T. Broadhurst, and K.-W. Huang, Contrasting galaxy formation from quantum wave dark matter, ψDM, with ΛCDM, using Planck and Hubble data, Astrophys. J. **818**, 89 (2016).
[163] R. Adam *et al.* (Planck Collaboration), Planck intermediate results. XLVII. Planck constraints on reionization history, arXiv:1605.03507.
[164] P. S. Corasaniti, S. Agarwal, D. J. E. Marsh, and S. Das, Constraints on dark matter scenarios from measurements of the galaxy luminosity function at high redshifts, arXiv:1611.05892.
[165] B. Bozek, D. J. E. Marsh, J. Silk, and R. F. G. Wyse, Galaxy UV-luminosity function and reionization constraints on axion dark matter, Mon. Not. R. Astron. Soc. **450**, 209 (2015).
[166] R. Cen, J. Miralda-Escude, J. P. Ostriker, and M. Rauch, Gravitational collapse of small scale structure as the origin of the Lyman-α forest, Astrophys. J. **437**, L9 (1994).
[167] L. Hernquist, N. Katz, D. H. Weinberg, and J. Miralda-Escude, The Lyman-α forest in the cold dark matter model, Astrophys. J. **457**, L51 (1996).
[168] Y. Zhang, P. Anninos, and M. L. Norman, A multi-species model for hydrogen and helium absorbers in Lyman-α forest clouds, Astrophys. J. **453**, L57 (1995).
[169] L. Hui, N. Y. Gnedin, and Y. Zhang, The statistics of density peaks and the column density distribution of the Lyman-α forest, Astrophys. J. **486**, 599 (1997).
[170] R. A. C. Croft, D. H. Weinberg, N. Katz, and L. Hernquist, Recovery of the power spectrum of mass fluctuations from observations of the Lyman-α forest, Astrophys. J. **495**, 44 (1998).
[171] N. Y. Gnedin and L. Hui, Probing the universe with the Lyman-α forest: 1. Hydrodynamics of the low density IGM, Mon. Not. R. Astron. Soc. **296**, 44 (1998).
[172] R. A. C. Croft, D. H. Weinberg, M. Pettini, L. Hernquist, and N. Katz, The power spectrum of mass fluctuations measured from the Lyman-α forest at redshift $z = 2.5$, Astrophys. J. **520**, 1 (1999).
[173] L. Hui, Recovery of the shape of the mass power spectrum from the Lyman-α forest, Astrophys. J. **516**, 519 (1999).
[174] L. Hui and N. Y. Gnedin, Equation of state of the photoionized intergalactic medium, Mon. Not. R. Astron. Soc. **292**, 27 (1997).
[175] P. McDonald, U. Seljak, R. Cen, P. Bode, and J. P. Ostriker, Physical effects on the Ly–α forest flux power spectrum: Damping wings, ionizing radiation fluctuations, and galactic winds, Mon. Not. R. Astron. Soc. **360**, 1471 (2005).

[176] R. A. C. Croft, Ionizing radiation fluctuations and large scale structure in the Lyman-α forest, Astrophys. J. **610**, 642 (2004).

[177] A. Meiksin and M. J. White, The effects of UV background correlations on Ly-α forest flux statistics, Mon. Not. R. Astron. Soc. **350**, 1107 (2004).

[178] L. Hui and Z. Haiman, The thermal memory of reionization history, Astrophys. J. **596**, 9 (2003).

[179] A. D'Aloisio, M. McQuinn, and H. Trac, Large opacity variations in the high-redshift Ly–α forest: The signature of relic temperature fluctuations from patchy reionization, Astrophys. J. **813**, L38 (2015).

[180] R. Cen, P. McDonald, H. Trac, and A. Loeb, Probing the epoch of reionization with the Lyman-α forest at $z \sim 4$–5, Astrophys. J. **706**, L164 (2009).

[181] N. Palanque-Delabrouille *et al.*, The one-dimensional Ly-α forest power spectrum from BOSS, Astron. Astrophys. **559**, A85 (2013).

[182] M. Zaldarriaga, L. Hui, and M. Tegmark, Constraints from the Lyman-α forest power spectrum, Astrophys. J. **557**, 519 (2001).

[183] M. Zaldarriaga, R. Scoccimarro, and L. Hui, Inferring the linear power spectrum from the Lyman-α forest, Astrophys. J. **590**, 1 (2003).

[184] A. Garzilli, A. Boyarsky, and O. Ruchayskiy, Cutoff in the Lyman alpha forest power spectrum: Warm IGM or warm dark matter?, arXiv:1510.07006.

[185] U. Seljak, A. Makarov, P. McDonald, and H. Trac, Can Sterile Neutrinos Be the Dark Matter?, Phys. Rev. Lett. **97**, 191303 (2006).

[186] J. Baur, N. Palanque-Delabrouille, C. Yèche, C. Magneville, and M. Viel, Lyman-α forests cool warm dark matter, arXiv:1512.01981.

[187] M. Viel, J. Schaye, and C. M. Booth, The impact of feedback from galaxy formation on the Lyman-α transmitted flux, Mon. Not. R. Astron. Soc. **429**, 1734 (2013).

[188] K. L. Adelberger, C. C. Steidel, A. E. Shapley, and M. Pettini, Galaxies and intergalactic matter at redshift $z \sim 3$: Overview, Astrophys. J. **584**, 45 (2003).

[189] P. van Dokkum, R. Abraham, J. Brodie, C. Conroy, S. Danieli, A. Merritt, L. Mowla, A. Romanowsky, and J. Zhang, A high stellar velocity dispersion and ~100 globular clusters for the ultra-diffuse galaxy Dragonfly 44, Astrophys. J. Lett. **828**, L6 (2016).

[190] D. H. Bernstein, E. Giladi, and K. R. W. Jones, Eigenstates of the general Schrödinger equation, Mod. Phys. Lett. A **13**, 2327 (1998).

[191] F. S. Guzmán and L. A. Ureña-López, Evolution of the Schrödinger-Newton system for a self-gravitating scalar field, Phys. Rev. D **69**, 124033 (2004).

[192] N. F. Mott and H. S. W. Massey, *The Theory of Atomic Collisions* (Clarendon Press, Oxford, 1949).

[193] V. G. Baryshevskii, I. D. Feranchuk, and P. B. Kats, Regularization of the Coulomb scattering problem, Phys. Rev. A **70**, 052701 (2004).

[194] E. Karule, Integrals of two confluent hypergeometric functions, J. Phys. A **23**, 1969 (1990).

[195] M. D. Weinberg, Self-gravitating response of a spherical galaxy to sinking satellites, Mon. Not. R. Astron. Soc. **239**, 549 (1989).